QUANTUM TUNNELING IN SOLID HYDROGEN

By

DAWEI ZHOU

A DISSERTATION PRESENTED
TO THE GRADUATE SCHOOL
OF THE UNIVERSITY OF FLORIDA IN
PARTIAL FULFILLMENT OF THE REQUIREMENTS
FOR THE DEGREE OF DOCTOR OF PHILOSOPHY

UNIVERSITY OF FLORIDA

1990

ACKNOWLEDGEMENTS

I would like to express my sincere and heartfelt appreciation to the many individuals who assisted and encouraged me to finish this dissertation that has taken six years mainly in the research laboratory

It is difficult to find words to describe the numerous contributions of my advisor Dr Neil S Sullivan As the chair of my supervisory committee he has always provided me direction guidance generous amounts of time of discussion with me and patience He spent countless hours teaching advising and helping me to think about the theoretical detail and giving me a big hand in the long period experiments in every detail He has always listened to suggestions and ideas from everyone in the group including me He has given me the opportunities to develop an independent research ability and he has always encouraged me to overcome the different kinds of difficulties In addition to helping me to accomplish my dissertation when I stood up to face difficulties I always felt that Dr Sullivan stood on my side when I was doing the right thing His spirit of devotion to science and his cooperation with colleagues and students has set a good example in my mind I want to say thanks to Dr Sullivan for all of his emotional support and encouragement

I express sincere appreciation to Professor R Pound of Harvard University He was kind to listen to me and to give me suggestions when he visited our laboratory for three months even though he is a physicist who is known worldwide

I am grateful to Professor H Meyer of Duke University for much kind guidance and discussion when he visited our laboratory when I visited Duke University and when meeting at professional conferences I would also like to thank Professors

E. R. Andrew, J. W. Dufty, and E. D. Adams, who gave excellent lectures during my graduate study and who always gave me help when I needed it.

I am also grateful to other members of my supervisory committee, Dr. K. N. Scott, Dr. J. R. Buchler, and Dr. S. Nagler, for their guidance and help.

It is my pleasure to thank Dr. Carl M. Edwards, who gave me much assistance with this dissertation. I want to say thank you to Dr. J. P. Brison, M. Rall, M. Parenti, M. Mauck, L. Couch, J. Rose, J. Kim, Y. S. Kim, J. S. Park, Dr. Y. Lin, Dr. P. M. Andersen, and everyone with whom I worked in the research laboratory.

I would like to thank Drs. G. Ihas, Y. Takano, M. Meisel, P. Wölfle, P. Kumar, D. A. Micha, B. L. Thomas, D. B. Tanner, S. Jeyadev, H. Van Rinsvelt, C. F. Hooper, Jr., F. Tobey, T. E. Walsh, and P. J. Hirschfeld for many discussions and assistance.

The help from low temperature laboratory engineers Chris Fombarlet, Don Sanford, Art Hingerty, and Greg Labbe; the help from the electronic shop engineers L. Phelps, J. Blitch, J. Legg, and L. Frederick; and the help from the mechanical shop, H. Nachtrieb, R. Spencer, B. Malphurs, J. Van Leer, J. Mynck, and S. Griffen, are greatly appreciated.

I would like to express my sincere thanks to the secretaries, Dorothea Roebuck, Kimberly Yocum, Patrick Tolley, Pauline Kirk, and others; without their warm help, I could not have finished my work.

The cooperation and friendship of my fellow graduate students, as well as that of the staff and faculty of the Department of Physics of the University of Florida, have made my stay as a graduate student at the University of Florida a pleasant and rewarding experience.

This research was supported by the National Science Foundation through Low Temperature Physics grants DMR-8611620, DMR-8913999 and the Division of Sponsored Research at the University of Florida

Finally, I would like to express my sincere appreciation to my parents, Dr Qi Zhou and Dr Yu Zhi Wang; they have overcome many difficulties to offer me a good educational opportunity; the price they paid cannot be counted. I am also very grateful for the unconditional support from my wife Penghua Wang, my son Xin Justin Zhou, my brothers Yalun Zhou and YaGe Zhou, and my sister Jingmei Zhou, without which I would not have been able to pursue my goals

TABLE OF CONTENTS

Page

ACKNOWLEDGEMENTS ii

ABSTRACT vii

1 INTRODUCTION 1

2 TUNNELING IN QUANTUM CRYSTALS 3
- 2.1 Quantum Crystals 3
- 2.2 Review of Tunneling in Solid He and Para-hydrogen 20
- 2.3 Introduction to Solid H_2 29
- 2.4 Feynman's Ring Exchange Model 33
- 2.5 Three Particle Quantum Tunneling Model in Solid *hcp* H_2 36
- 2.6 Observation of Quantum Tunneling in Solid H_2 and the Importance of H_2 Studies 41

3 NUCLEAR SPIN RELAXATION IN THE PRESENCE OF TUNNELING 44
- 3.1 Overview of the Relaxation of HD Impurities in Solid H_2 44
- 3.2 Vacancy-Induced Nuclear Spin-Lattice Relaxation in Solid H_2 50

4 EXPERIMENTAL APPARATUS 58
- 4.1 Cryogenics 58
- 4.2 NMR Sample Cell 60
- 4.3 Pulsed NMR Apparatus 60
- 4.4 Continuous Wave (CW) NMR Apparatus 62
- 4.5 Precise and Efficient In-Situ Ortho-Para Hydrogen Converter 65
- 4.6 Pressure Gauge and Pressure Detector 66
- 4.7 Data Acquisition 68

5 EXPERIMENTAL RESULTS AND DISCUSSION 71
- 5.1 Sample Preparation 71
- 5.2 Pulse NMR Sequence 73
- 5.3 Temperature Dependence of T_2 74

5.4 Temperature Dependence of T_1 79
5.5 Pressure Dependence of T_2 86
5.6 Clustering of the Ortho H_2 92

6 SUMMARY AND CONCLUSIONS 93

APPENDIX A 99

APPENDIX B 101

REFERENCES 105

BIOGRAPHICAL SKETCH 109

Abstract of Dissertation Presented to the Graduate School
of the University of Florida in Partial Fulfillment of the
Requirements for the Degree of Doctor of Philosophy

QUANTUM TUNNELING IN SOLID HYDROGEN

By

DAWEI ZHOU

May 1990

Chairman: Neil S. Sullivan
Major Department: Physics

The distinguishing property of quantum crystals such as solid helium and solid hydrogen is the large zero-point motion of the molecules about their equilibrium positions. The origins of the large zero-point motion in quantum crystals are the small molecular mass, the large kinetic energy, and the very shallow effective potential well. There is an appreciable overlap of the wave functions of the molecules on neighboring lattice sites as a result of the zero point motion and this allows particles and defects such as vacancies or isotopic impurities to exchange positions with nearest neighbor molecules in a coherent manner. The nature of the coherent exchange processes in solid ^{3}He are now believed to include three- and four-particle cyclic permutations. It has been argued that the exchange is determined by the available free volume for permuting the particles, and this qualitatively explains the dominance of three- and four-particle exchange over two-particle permutations in bcc ^{3}He.

It is important to check whether the multi-particle cyclic permutation model works for solid H_2 — another family member of quantum crystals. Such measurements would provide a severe test of the multiple-exchange model because of the very large difference between conventional two-particle and three-particle exchange in solid hydrogen. (This difference of ~ 4 orders of magnitude does not

occur for solid helium.) Delrieu and Sullivan predict a three-particle exchange rate (~1 kHz) in *hcp* H_2 at normal densities. This rate is at least four orders of magnitude higher than the calculations for the two-particle exchange model ($10^{-1} - 10^{-4}$ Hz).

This dissertation has carried out the NMR experiments to test the multiple exchange model in solid H_2. The NMR experimental results are the following:

(1) The HD impurity (or para H_2) tunneling frequencies are 1.5 kHz at low temperatures below 6K, i.e., in the order of 1 kHz.

(2) The tunneling frequency is pressure dependent.

(3) NMR transverse relaxation results are consistent with a model for the vacancy motion which predicts that there are two different kinds of motions:

   a) classical hopping at high temperatures, and

   b) quantum tunneling at low temperatures.

CHAPTER 1

INTRODUCTION

There are two species of hydrogen molecules. One is ortho hydrogen molecule with total nuclear spin $I = 1$, odd molecular angular momentum ($J = 1$ at low temperatures). The other species is para hydrogen with total nuclear spin $I = 0$, even molecular angular momentum ($J = 0$ at low temperatures). There is a strong electric quadrupole-quadrupole interaction EQQ between ortho hydrogen molecules in solid hydrogen, and as a result the tunneling of ortho-hydrogen molecules is quenched in solid hydrogen at low temperatures. In contrast to the ortho-hydrogen, the spherically symmetric para hydrogens can exchange positions with nearest neighbors very easily due to the overlap of wave functions. There are some open questions as follows:

Do para hydrogen molecules exchange positions by two particle exchange or by three- particle cyclic exchange in solid hydrogen at low temperatures? How does one test for tunneling of a para hydrogen molecule, which has total nuclear spin $I = 0$, by NMR experiments?

Does quantum tunneling occur for vacancies in solid hydrogen?

This dissertation is going to answer the above questions.

The distinguishing property of quantum crystals, such as solid helium and solid hydrogen, is the large zero-point motion of the molecules about their equilibrium positions. There is an appreciable overlap of the wave functions of the molecules on neighboring lattice sites, and this allows particles and defects such as vacancies or isotopic impurities to exchange positions with nearest neighbor molecules. Classically, such defects are regarded as localized objects which move only occasionally by thermal excitation over intervening potential energy barriers. In quantum crystals, Andreev and Lifshitz[1] have predicted that the defects will become delocalized and move through the crystal in a coherent manner. Convincing evidence for coherent impuriton motion of ^{3}He impurities in solid *hcp* ^{4}He has been obtained by NMR measurements[2,3] of the self diffusion constant D and the nuclear transverse relaxation time T_2 for very low impurity concentrations ($x < 5 \times 10^{-4}$).

The nature of the exchange processes in solid ^{3}He (which are now believed to include three- and four-particle cyclic permutations) determines the phase diagram and detailed structures of the nuclear magnetically ordered states. It has been argued that the exchange is determined by the available free volume for permuting the particles in the solid, and this qualitatively explains the dominance of three- and four-particle exchange over two-particle permutations in *bcc* ^{3}He. The same model predicts an unexpectedly large three-particle exchange rate (~ 1 kHz) in *hcp* H_2 at normal densities, and an exchange frequency dependence on pressure; observation of such rates would provide a severe test of the multiple exchange model.

We have carried out studies of the proton nuclear spin-spin relaxation T_2 and the spin-lattice relaxation T_1 of HD impurities in order to test for the existence of quantum tunneling of HD impurities whose ground states are spherically symmetric and can participate in exchange processes with the para-hydrogen molecules, and thus be used by NMR as a probe to test for the existence of classical hopping and quantum tunneling of vacancies in solid hydrogen.

CHAPTER 2

TUNNELING IN QUANTUM CRYSTALS

2.1 Quantum Crystals

Quantum crystals are defined as crystals in which the zero point amplitude of an atom about its equilibrium position is a large fraction of the intermolecular distance R_0. The *rms* displacement $< u^2 >^{\frac{1}{2}}$ of molecules is as large as $0.33R_0$ in solid He and as large as $0.18R_0$ in solid H_2 at low temperatures. The large zero point motion is a consequence of the small molecular mass and the weakness of the attractive interaction between nearest neighbor molecules. Although all solids show quantum effects to a certain degree, quantum crystals made from the lightest elements (^3He, ^4He, H_2, D_2, ...) have special properties of purely quantum mechanical origin that set them apart.

2.1.1 Main Character of Quantum Crystals

2.1.1.1 Weak localization

The important property of the quantum crystals is that the constituent atoms (or molecules) are only weakly localized with respect to quantum zero point motion (ZPM). Because the particles have only small mass and because the cohesive forces are very weak, the kinetic energy is large, and there is therefore a large amplitude of zero point motion, i.e., the deviations about the equilibrium position are a sizeable fraction of the nearest neighbor separation.

2.1.1.2 Correlations and coherent motion

As the molecules move away from their lattice sites they tend to encounter other atoms and experience strong repulsive interactions if they come close to one another. This is called hard core repulsion and has as its origin the Pauli exclusion principle which comes into play when the electronic charge distributions start to overlap. The motions in the N particle system therefore tend to be correlated to avoid nearest neighbor encounters. These are short range correlations and imply that the multi-particle cyclic permutations may minimize the Gibbs free energy in the quantum crystals.

2.1.1.3 Exchange mechanism

As an atom moves, another neighboring atom may move into the 'vacant' lattice site left by the first atom which in its turn can tumble into the 'hole' created by the second atom. The exchange probability is proportional to the overlap of the wave functions of the particles.

By the Pauli principle the nearest neighbor atoms must stay at least a distance a (hard core) away. Thus the motion of the atom and its neighbor is correlated and the exchange will therefore almost certainly involve a group of atoms rather than just a pair. In the light of modern theories three particle and 4 particle ring exchange is expected to be more important than ordinary two particle exchange in solid ^{3}He and other quantum crystals such as solid hydrogen. We will discuss the exchange mechanism in detail later.

2.1.2 Elementary Quantum Theory of Corresponding States

2.1.2.1 Lennard-Jones potential

We first consider the problem of N particles in a crystal with Hamiltonian

$$H = -\frac{\hbar^2}{2m}\sum_i \nabla_i^2 + \sum_{i<j} V(r_{ij}) \tag{1}$$

$V(r_{ij})$ is an atom-atom pair potential and the $\sum_{i<j}$ is over all distinct pairs. Although it is in principle possible $V(r)$ has not yet been calculated because of

the difficulty and phenomenological forms are used. The most familiar form is the Lennard Jones potential

$$V(r) = 4\epsilon[(\frac{\sigma}{r})^{12} - (\frac{\sigma}{r})^{6}] \tag{2}$$

The parameters ϵ, σ are determined from experimental measurements of the virial coefficients of gases which are sensitive to atom-atom scattering processes. The Lennard Jones form is illustrated in Fig. 1

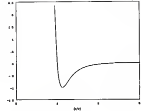

Figure 1 Lennard-Jones Potential. Ref. 41

The potential $V(r)$ has two contributions: an attractive $\frac{1}{r^6}$ [illegible] strong $\frac{1}{r^{12}}$ repulsive potential.

(1) The attractive component is due to the indirect induced electric dipole-dipole interaction. There is no permanent dipole but an instantaneous dipole can be created by a fluctuation; this dipole creates an electric field which in turn induces a dipole in a second atom and hence the interaction between the induced dipole and the fluctuation created dipole.

(2) The repulsive component of the potential results from the Pauli exclusion principle when the electronic charge distribution of the two atoms begin to overlap at short distances. The potential $V(r) = 0$ at $r = \sigma$ and $\epsilon = -V(r_0) = V_0$ where the V_0 is the potential energy of an atom localized at the potential well minimum $(r = r_0)$.

2.1.2.2 de Boer quantum parameter

One parameter that needs to be estimated in order to establish the relative importance of the amplitude of zero point motion for different atoms and in order to distinguish the quantum crystals and the classical crystals is the mean square fluctuation $\langle u^2\rangle$ about the average position. The instantaneous position $\vec{r}_i = \vec{R}_i + \vec{u}_i$ where $\vec{R}_i$ defines the position of a lattice site and $\vec{u}_i$ is the displacement from a lattice site. We will see later that there is a one to one correspondence between the r.m.s. displacement $\langle u^2\rangle^{\frac{1}{2}}$ and the quantum parameter Λ introduced by de Boer. If one introduces $r^* = \frac{r}{\sigma}$ and $V^* = \frac{V}{\epsilon}$ in the potential, then $V_{ij}^* = \epsilon(r_{ij}^{-12} - r_{ij}^{-6})$ and the Schrodinger equation

$$(-\frac{\hbar^2}{2m}\nabla^2 + \sum_{i<j} V_{ij})\Psi = E\Psi \tag{3}$$

becomes

$$(-\Lambda^2(\nabla^*)^2 + V^*)\Psi = E^*\Psi \tag{4}$$

where $(\nabla^*)^2$ is an abbreviation for $\sum_i \nabla_i^{*2}$ and

$$\Lambda = \frac{\hbar}{\sqrt{2m\epsilon_0\sigma^2}}$$

is the de Boer quantum parameter

We can see that Λ is inversely proportional to the $\sqrt{m}$ and $\sqrt{\epsilon_0}$ this mean that the smaller the mass of an atom the larger the de Boer parameter, and the shallower the potential well the larger the value which corresponds to larger zero point motion. The de Boer parameter Λ is therefore a measure of the zero point motion of an atom that can be used to distinguish the quantum crystals and the classical crystals.

The point of this approach is to reduce the potential to a common form by rescaling and see what the consequences are for the expectation values of the kinetic energy $< -\Lambda^2(\nabla^*)^2 >$. The relative displacement $< u^2 >^{\frac{1}{2}}$ is plotted as a function of the quantum parameter Λ in Fig. 2.

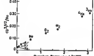

Figure 2. The theoretical *rms* zero point displacement amplitude relative to the nearest neighbor distances for a number of light solids. Ref. 5.

As can be seen from the figure the deviation is as high as 33% of the lattice spacing a_0 for the helium isotopes and as high as 18% of the lattice spacing a_0 for hydrogen. The relevant potential parameters and length scales are collected in Table 1.

Table 1. Typical Lengths

	m (amu)	a_0 (Å)	ϵ (degK)	σ (Å)	σ/a_0	Λ (Å)
^{3}He	3.016	0.93	10.2	2.56	2.75	3.08
^{4}He	4.003	0.93	10.2	2.56	2.75	2.67
H_2	2.016	1.11	37.0	2.92	2.63	1.74
Ne	20.2	1.17	35.6	2.72	2.41	0.44
Ar	40	1.54	119	3.43	2.24	0.12
Kr	84	1.69	139	3.60	2.13	0.06
Xe	131	1.90	228	3.97	2.09	0.04

$\Lambda = h/\sqrt{(2m\epsilon\sigma^2)}$ De Boer's Parameter. m = mass, a_0 = lattice spacing, ϵ = potential well depth

The potential for some of the lighter rare gases are illustrated in Fig. 3, and one point is immediately clear.

The He–He potential is flat and shallow with small curvature compared to the heavier rare gases. The amplitude of the oscillation can therefore be large for He compared to Xe. This is due to the fact that Xe has a deep potential well with a high curvature $V''(r)$ at the bottom of the well, and thus a strong restoring force for small oscillations about the well minimum.

2.1.2.3 Large ZPM (zero point motion) and the phase diagrams of helium

The large ZPM is the unique character of quantum solids and quantum liquids. The first striking consequence of the large ZPM is that the helium isotopes

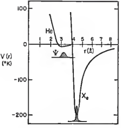

Figure 3 Comparison of atom-atom potentials V (r) and spread of wave function ψ_0 for He and Xe, quantum crystal and classical crystal respectively

^{3}He and ^{4}He do not solidify without applied pressure The (P T) phase diagrams are shown in Fig 4

We can see that ^{4}He has four properties which are direct consequences of the ZPM

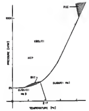

Figure 4a. Phase diagram for ^{4}He

(1) It is a liquid at $T = 0$ for applied pressures $p < 25$ atmospheres and a superfluid for $T < 2.17$ K

(2) It forms an *hcp* solid with 12 nearest neighbors for $25 < P < 1000$ atmospheres

(3) The solid is *fcc* for $P > 10\ 000$ atmospheres

The properties of ^{3}He that are direct consequences of the ZPM are as follows

(1) A liquid at $T = 0$ for $P < 34$ atmospheres

(2) A degenerate Fermi liquid for $T < 0.3$K and superfluid phases occur for $T < 3$mK

(3) A *bcc* solid for $29.5 < P < 100$ atmospheres

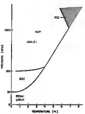

Figure 4b Phase diagram for ^{3}He

(4) A *hcp* solid for $100 < P < 1000$ atmospheres

(5) A *fcc* solid for $P > 1000$ atmospheres

The solid heliums are the only dielectric solids which crystallize in a *bcc* phase. This is directly linked to the ZPM and is purely quantum mechanical in origin.[4] Another important point is that solid helium is the softest solid that occurs in nature. The rate $\frac{\partial l}{\partial P}$ is the largest for all solids, i.e. a large change in interatomic spacing is observed for moderate applied pressure. This is illustrated in Table II

Table II. Variation of molar volume V_m (cc/mole) of solid ^{3}He with applied pressure

V_m	P(bars)
17.63 (hcp)	195
23.05 (bcc)	43

2.1.3 Why Do We Call the Solid Heliums and Solid Hydrogen Quantum Crystals

2.1.3.1 Shallow potential well

If we consider the Leannard–Jones potential the potential energy V_0 of an atom localized at the potential well minimum ($r = r_0$) is

$$V_0 = V(r_0) = -\epsilon$$

and for z nearest neighbors

$$V_0 = -z\epsilon$$

We can consider small oscillations about $r = r_0$ by expanding $V(r)$ in a Taylor series

$$V(u) = V_0 + \frac{1}{2}V''(r_0)u^2 + \qquad (6)$$

where $V''(r_0)$ is the curvature of the minimum. The total kinetic energy of motion for simple harmonic oscillations about r_0 is $<T>= \frac{3}{2}\hbar\omega_0$ where the natural frequency $\omega_0 = \sqrt{\frac{k}{m}}$ and the stiffness constant

$$k = V''(r_0) \qquad (7)$$

Since one half of the potential energy is shared by neighbors, the total dynamic energy

$$E_{dyn} = <T> + \frac{1}{2} <PE> = \frac{9}{8}\hbar\left(\frac{V''(r_0)}{m}\right)^{\frac{1}{2}} \qquad (8)$$

The total energy can be calculated for this simple case of oscillations in the bottom of the well using the Lennard-Jones parameters The results are given in Table III and we make the striking observation that the total energy is positive for solid helium This means that solid ^{3}He will not form if the atom atom interactions are the only source of attractive binding We have to apply external pressure to obtain solid helium otherwise it will remain liquid at low temperatures even when the temperatures approach absolute zero Kelvin

Table III Typical energies (units 0° K)

	ϵ	$\frac{1}{2}V_0$	E_{dyn}	E_{TOT}^{CAL}	E_{TOT}^{EXP}
He	10	-41	101	+ 66	1
Ne	36	-220	82	-138	-225
Ar	119	715	147	568	930
Xe	220	1370	57	1313	1920

Where the ϵ is the depth of the potential well $V_0 = -\epsilon$ is the average potential energy the E_{dyn} is the dynamical energy the E_{TOT}^{CAL} is the total energy calculated for small oscillations and the E_{total}^{exp} is an experimental total energy deduced from heats of sublimation

2 1 3.2 Weak localization, large kinetic energy and large spreading of wave function

To simplify we attempt to obtain an elementary view of the problem of localization and calculate the kinetic energy of localization by solving the Schrodinger equation assuming simple Gaussian wave functions

$$\Phi(u) = e^{-\frac{1}{2}\alpha^2 u^2} \tag{9}$$

for each particle and neglecting all correlations

We take the total crystal wave function to be the simple product $\Phi = \prod_i \phi_i(u)$ and treat the particles as independent The Schrodinger equation

$$(\frac{1}{2m}p^2 + \frac{1}{2}ku^2)\phi(u) = E\phi(u) \tag{10}$$

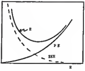

Figure 5 Comparison of Zero Point Kinetic Energy (ZKE) with Potential Energy (PE) Ref 24

satisfies the Gaussian form for $k = \frac{\hbar^2\alpha^4}{m}$ The kinetic energy of the harmonic oscillatory motion is

$$\langle T\rangle = \frac{3}{2}\frac{\hbar^2\alpha^2}{m} \tag{11}$$

and the total dynamic energy is

$$E_{dyn} = \frac{9}{8}\frac{\hbar^2\alpha^2}{m} \tag{12}$$

Now define W as the width of the density of the wave function that describes the spread of the $|\varphi|^2$ (density of wave function) in space The W will describe the degree of localization of the atom on the lattice The large W is corresponding to the large probability of finding the atom relatively far from its lattice site For the Gaussian wave function of equation (9)

$$W = \frac{1}{\alpha}$$

From equation (12), we find that the kinetic energy varies as

$$\langle T\rangle \propto \frac{1}{m\mathfrak{H}^2}$$

and the potential energy evaluated using the Gaussian wave functions will vary as

$$|P.E.| \sim \mathfrak{H}^2$$

The width of the wave function (which is a measure of the spatial extension of ϕ) is therefore determined by two competing factors

(1) the ZPM "kinetic" energy $\langle T\rangle \propto \frac{1}{m\mathfrak{H}^2}$ as opposed to

(2) the potential energy $|P.E.| \propto \mathfrak{H}^2$

Because of the small mass of the quantum crystals, the largest amplitude zero point motion (related to $\mathfrak{H}$) may minimize the total energy. Because the large kinetic energy of quantum crystals, the position of minimum of total energy $(\langle T\rangle + \langle P.E.\rangle)$ R_1 is larger than R_0, where the R_0 is the position of the minimum of the potential energy and the wave function of quantum crystal is wider than classical crystal. This can be seen in Fig. 3, Fig. 6, and Fig. 7.

The degree of localization or r.m.s. deviation $\langle u^2\rangle^{\frac{1}{2}}$ can be calculated using the Gaussian wave function

$$\langle u^2\rangle = \frac{3}{2}\frac{1}{\alpha^2} = \frac{3\hbar}{2}\left(\frac{2}{m\mathfrak{V}''}\right)^{\frac{1}{2}} \qquad (13)$$

The r.m.s. deviation increases as m decreases, and also as the well curvature $\mathfrak{V}''$ decreases, and therefore the degree of the localization decreases and the wave functions spread out rapidly for lighter masses and shallow potentials. The results of the calculations of $\langle u^2\rangle^{\frac{1}{2}}$ for the light rare gases and H_2 are collected in Table IV and compared with the other characteristic lengths.

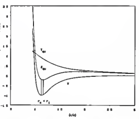

Figure 6 Energy curves for quantum solids. The r_1 is the position of minimum of total energy and the r_0 is the position of minimum of potential energy. Ref 41

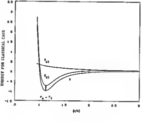

Figure 7 Energy situation for classical solids $r_0 \sim r_1$. Ref. 41

Table IV. Comparison of r.m.s. deviation $\langle u^2\rangle^{\frac{1}{2}}$ with other lengths: at $\sigma = r$ the potential $V(r) = 0$; r_0 the well depth minimum and δ the nearest neighbor separation. The $\langle u^2\rangle_D$ is calculated using the standard Debye approximation.

	$\langle\sigma\rangle$	$R_0 = 2^{\frac{1}{6}}\sigma$	δ	$\langle u^2\rangle^{\frac{1}{2}}$	$\frac{\delta-2\langle u^2\rangle^{\frac{1}{2}}}{\sigma}$	$\langle u^2\rangle_D$
He	2.56	2.86	3.77	0.42	0.98	1.15
H_2	2.92	3.63	3.75	0.31	1.0	0.33
Ne	2.82	3.16	3.16	0.29	1.01	0.27
Ar	3.45	3.87	3.76	0.15	1.03	0.16
Kr	3.98	4.46	4.33	0.10	1.05	0.11
Xe	3.61	4.04	3.99	0.12	1.06	0.13

2.1.3.3 Hard core model

Considerable insight into the nature of quantum solids can be obtained by a simple calculation of the ground state energy of a hard sphere model. This is described by Guyer [5]. In this model, each atom is viewed as carrying a hard core (radius $\nu = 0.8368\sigma$) and occupying a volume $\frac{4\pi}{3}(\sigma+\alpha^{-1})^3$ where α^{-1} is a measure of the width of the wave function. The conclusions from this model are consistent with the previous analysis, i.e. the atoms are too light and the attractive interactions are too weak for the atom to reside at r_0, the minimum of the pair potential. It is not possible to simply increase the spread in the wave function $\phi(u)$ with $\phi(u)$ centered at r_0 because the atoms will then feel the repulsive interactions with their neighbors. It is therefore necessary to expand the lattice to $R_l > R_0$. At such conditions, to increase the width of $\phi(u)$ it becomes possible and to minimize the total energy. As a result of this need to expand $\phi(u)$, the particle can do work against the attractive pair potential and without a constraining experimental pressure the system remains liquid for helium.

2.1.4 Practical Consequences of Zero Point Motion

The large amplitude zero point motion for quantum crystals results in several important practical consequences as follows:

1. External pressure is needed to obtain the solid phase for helium.

2. At low pressures it is easier to avoid nearest neighbor encounters, and thus the hard core repulsions, if the atoms arrange themselves in a bcc lattice. This is unique to solid ^{3}He and solid ^{4}He.

3. The pure single crystals of high quality of solid He and solid H_2 can be grown easily and rapidly (1 cm/min rates can be achieved). The crystals are soft and in a sense, self annealing. This results from the fact that ZPM allows for some repairing of local crystal defects very quickly. It is easy to understand the lack of dislocations and surface defects in the quantum crystals.

4. Point defects or vacancies of the Schottky type should be highly mobile since there will be a high probability that an atom with its zero point motion will move into a vacant site. This motion results in an effective quantum mechanical tunneling of the atoms through the crystals. The vacancies are therefore delocalized, they are not to be regarded as point defects, and they should propagate as waves. This vacancy wave motion has been sought for by NMR experiments which are very sensitive to the motion of atoms. The experiments before ours have not been sufficiently precise to distinguish between the quantum tunneling and the classical hopping of vacancies in the quantum crystals.

5. The large ZPM and the hard core potential established the strong correlation between the atoms, and thus results in the particle-particle exchange in a coherent matter, i.e., multiple cyclic permutation rather than pair exchange dominates the exchange process in the quantum crystals. We will discuss this in detail later.

6 The Gaussian approximation only can be used to do the energy calculations and it cannot be use to calculate the overlap of the wave functions A new theory is needed to carry this out

2 1.5 Summary

The qualitative discussion we have developed in comparing classical solids to the quantum solids can be summarized as follows

(1) The kinetic energy $\langle T\rangle$ is comparable to the magnitude of the potential energy $|\langle V\rangle|$ the minimum in the total energy $E_{total} = \langle T\rangle + \langle V\rangle$ occurs for values of $r > r_0$ the minimum of V_{pair} (2) There is a large spreading the wave function and the particles are poorly localized i e there is a large amplitude of zero point motion resulting in a quantum tunneling motion in a coherent matter

And the quantum crystals therefore appear to be less dense than if they were behaving classically

2.2 Review of Tunneling in Solid He and Para-hydrogen

We have seen above that one of the most dramatic consequences of the zero point motion in quantum crystals is the particle particle exchange whose rate is proportional to the overlap of the wave functions

The exchange mechanisms in quantum crystals are very different from those of classical crystals In the quantum crystals not only the electrons but the whole atoms, electrons and nuclei exchange places Such exchanges are dominated by three or four-particle cyclic permutations rather than two-particle exchange i e such exchanges occur in a coherent matter to minimize the exchange activation energy and to satisfy the limited free space in the quantum crystal. To illustrate this, think of the following picture Suppose you are traveling at rush hour in the subway —the crowd is so dense that people can hardly move It is practically impossible to exchange positions with one of your nearest neighbors only without disturbing the others. But this exchange will be practical if you do three- or four-body cyclic permutations, because such motion requires less free space and less activation energy. This is exactly the situation in a hard-sphere quantum solid at large densities.

2.2.1 Review of the Pairwise Exchange Model

The earliest theories of exchange [6] considered only the exchange of two nearest neighbors. Gaussian wave functions $\phi(\vec{r}-\vec{R}_i) = (\frac{A}{\pi})^{\frac{3}{4}} \exp[-\frac{1}{2}A(r-R_i)^2]$ were assumed for an atom associated with lattice site i. The exchange energy is determined by solving the two particle problem. The symmetric and the antisymmetric wave functions have eigenvalues E_s and E_a, respectively. The exchange frequency is defined as

$$J_{pair} = \frac{E_s - E_a}{2\hbar}$$

and can be shown to be given by the overlap integral

$$J_{pair} = \frac{\hbar A}{m}\frac{AR_0^2}{2\pi}\exp[-\frac{1}{2}A(R_0^2 + a^2)] \tag{14}$$

where R_0 is the nearest neighbor separation and a the hard core radius. A is estimated from the Debye approximation for the kinetic energy

$$\langle T\rangle = \frac{3}{4}\frac{\hbar A}{m} = \frac{\hbar}{2}\Omega_D$$

This simple estimate for J provides not only the right order of magnitude, but it also predicts the correct density dependence at high temperatures. However, the simple Heisenberg exchange Hamiltonian was inadequate at low temperatures. Careful measurements of the pressure as a function of temperature and applied magnetic field by Kirk and Adams[7] showed significant deviations from the predictions of a simple Heisenberg model. The nuclear spin susceptibility χ was also found to be larger than the Curie-Weiss law below 10 mk. It was also discovered that the transition to the ordered nuclear spin state was first order, which is opposed to the second order transition predicted by the Heisenberg model.

Because the pairwise exchange model failed at low temperature, we need a better theoretical model for the exchange in quantum crystals.

2.2.2 Calculation of Triple Exchange in Dense *hcp* ^{3}He and Para-hydrogen

A short time after the observation of the magnetic ordering, Hetherington and Willard[8] showed that large ring-exchange terms can account for the first order transition at 1 mk and give qualitatively the shape of the phase diagram. Roger, Hetherington, and Delrieu[9,10] found that they could account for the unexpected results for the ordered states of solid ^{3}He if they introduced three- and four-particle exchange mechanisms in addition to pairwise exchange. J.M. Delrieu and N.S. Sullivan[11] extended the model to solid para-hydrogen and expected an exchange frequency as high as 1 KHz to compare with $10^{-3} - 10^{-4}$ Hz expected by the pairwise exchange model, which needs to be tested by experiments.

We will now consider the multiple exchange in more detail. In the ring exchange demonstrated in Fig. 8, three atoms initially localized near sites i, j, k cycle in a clockwise or counterclockwise fashion.

The exchange rate at which this permutation occurs is limited by the strong repulsive short range interactions between the permuting atoms in the midway position (shown by the dotted circles) and the nearest neighbors of the surrounding atoms. The interaction of permutation is described by an effective potential V_{eff} and it limits the path to a narrow duct (Fig. 12) in the configuration space.

In the 3N-dimensional configuration space, the orbital wave function $\phi(\vec{r})$, $\vec{r} = (\vec{r}_1, \vec{r}_2, \ldots, \vec{r}_N)$, takes appreciable values only when each particle i is near its lattice site $\vec{R}_i$. We give the name "cavity" to a region of configuration space

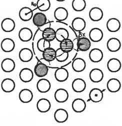

Figure 8. Schematic representation of a 3-particle exchange in an *hcp* lattice. The displacement of the nearest neighbors to the permuting triad of atoms is designated by δX. Ref. 11.

where the probability $\phi^2(\vec{r})$ for the wave function is high. For a system of N identical but distinguishable particles, there are $N!$ ways to assign N particles to N lattice sites. Thus, we define $N!$ cavities Ω_p, each containing configurations in which each particle i is near the lattice site $\vec{R}_{p(i)}$.

These cavities are connected by regions of small but finite probability for the wave function called "ducts."

In order to determine the potential V_{eff} during the cyclic ring exchange we adopt the Delrieu and Sullivan model. We consider three atoms tunneling in the

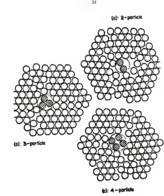

Figure 8 Illustration of the perturbation of surrounding lattice by (a) 2 particle (b) 3-particle and (c) 4-particle cyclic permutations of hard discs on a triangular lattice As the density is reduced beyond that for the triangular close packing 3 particle cyclic exchange is the first type to be allowed

(100) plane of an *hcp* lattice as shown in Fig 8 The relative sizes of the circles in Fig 8 refer to a hard sphere model for solid para hydrogen for which the ratio (R_0/σ) of the nearest neighbor separation R_0 to the hard core diameter σ

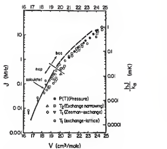

Figure 10 Comparison of calculated exchange rates with observed values for solid ^{3}He as a function of molar volume

is 1.5 The three permuting atoms in the center of the figure are maintained at the equilibrium distance R_0 from each other. They turn on a circle of radius $R_0/\sqrt{3}$. The three surrounding atoms shown in bold face are the atoms in which interact strongly with the cycling atoms during the permutation. We consider the "adiabatic" limit in which the surrounding medium (beyond the bold faced atoms) can deform elastically in order to minimize the total potential energy. The obvious constraint is that the atoms in the immediate neighborhood of the cycling

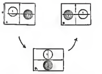

Figure 11 Physical illustration of configurations in Figure 14 A is one probable configuration with particles 1 and 2 in the L.H.S and R.H.S boxes configuration D represents an improbable intermediate position corresponding to tunneling from configuration A to B Configurations such as D correspond to points in the duct $L(t)$ of Figure 12 Ref 24

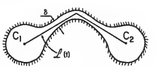

Figure 12 Configuration space showing two cavities C_1 and C_2 of high probability and a narrow exchange duct connecting the configurations Ref 24

atoms move so that the mean separation R_0 is maintained between them and the exchanging atoms The three bold faced atoms must move away a distance

$$\delta(x) = (1 - \frac{1}{\sqrt{3}})R_0 \tag{15}$$

The volume taken up by the exchanging atoms is taken that of a cylinder of radius

$$R = (\frac{1}{2} + \frac{1}{\sqrt{3}})R_0 \qquad (16a)$$

and

$$h_0 = (\frac{2}{3})^{\frac{1}{2}} R_0 \qquad (16b)$$

which is the height of the cylinder occupied by each atom in equilibrium in the *hcp* lattice

In the absence of exchange motion the volume V_0 of the three atoms is

$$V_0 = \frac{3}{\sqrt{2}} R_0^3 = 3V_m \qquad (17)$$

where V_m is the molar volume The increase in volume required during the exchange is therefore

$$\Delta V = V - V_0 = \pi R^2 h_0 - V_0 = 1.21 V_m \qquad (18)$$

The effective potential energy can be obtained by

$$\delta U = \int_{V_0}^{V_0+\Delta V} P dV = -P\Delta V + \frac{1}{\beta}(\Delta V)^2/V_0 \qquad (19)$$

where P is the pressure and

$$\beta = -\frac{1}{V}\frac{\partial V}{\partial P}$$

is the compressibility at $T = 0$ Delrieu and Sullivan used the experimental values.[12,13] the error bar of the experiments leaves an uncertainty in the value of δU, and this will effect the results of calculation but they will be good to an order of magnitude

Assuming the effective potential in the configuration space V_{eff} which is related to the δU in equation (19) can be written as Fig 10

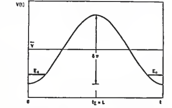

Figure 13 Approximate form for the tunneling as a function of the distance t in configuration space The point $t = t_\Sigma$ corresponds to the configuration shown in Fig 8 for which the permuting particles are in positions of closest approach to their neighbors (This corresponds to the center of the duct connecting the two cavities in configuration space)

$$V_{eff}(t) = -\frac{1}{2}\delta V \cos\frac{\pi t}{L} + \bar{V} \tag{20}$$

For this simple sinusoidal form for V_{eff} the one dimensional Schrodinger equation turns out to be Mathieu s equation

$$\frac{d^2y}{dV^2} + (a - 2q\cos 2V)y = 0 \tag{21}$$

for the variables

$$V = \frac{\pi t}{2L} \text{and} \quad q = -\frac{2mL^2\delta V}{\pi^2\hbar^2} \tag{22}$$

The solutions of Mathieu s equation can be found in Abramowitz and Stegun[14] and in terms of their lowest eigen solutions b_1 and a_0 the exchange frequency

$$2\hbar J = \frac{\hbar^2}{2m}\left(\frac{\pi}{2L}\right)^2 (b_1 - a_0) = 2^5\left(\frac{2}{\pi}\right)^{\frac{1}{2}}\frac{\hbar^2}{2m}\,\frac{\pi^2}{4L^2}\,q^{\frac{3}{4}}e^{-4\sqrt{q}} \tag{23}$$

The tunneling Hamiltonian is

$$H = J\Sigma P_{ijk}$$

where P_{ijk} is the corresponding three particle cyclic permutation operator. The exchange length L is the sum of the square of the displacements in Fig. 8 and $L^2 = \sum_i(\delta X_i)^2$. The displacements are contributed by (a) the motion of the three exchange atoms as they move on a circle of radius

$$(R - \frac{1}{2}R_0) = R_0/\sqrt{3} \tag{24}$$

with an angular displacement $\pi/3$ giving $L_0^2 = 3(\frac{\pi}{3}\frac{R_0}{\sqrt{3}})^2$ and (b) the displacement of the surrounding atoms, essentially that of the three bold faced neighbors in Fig. 8 which each move

$$\delta x = (1 - \frac{1}{\sqrt{3}})R_0 \tag{25}$$

In order to take into account the compressibility of the surrounding medium this is reduced to $0.86\delta x$. The total path length in the configuration space is therefore

$$L = [L_0^2 + 3(0.86\delta x)^2]^{\frac{1}{2}} = 1.2R_0 \tag{26}$$

Calculating L for a given R_0 (i.e. a given density) and using the experimental data for the compressibility we can find δL and then g and evaluate the exchange frequency J_3 for 3 particle ring exchange. The results of the calculation for solid ^{3}He are shown in Fig. 10 and compared with the experimental values.

The agreement is remarkably good, given the assumptions made in the model. Let us move to another candidate of quantum crystals — solid hydrogen.

2.3 Introduction to Solid H_2

Solid hydrogen is a remarkable subject for study from both theoretical and experimental viewpoints.[13] The origin of this interest is that both the translational

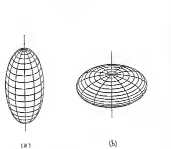

Figure 14a and Figure 14b Orientational degrees of freedom of an ortho hydrogen molecule — an ellipsoid (a) orientation number $\sigma > 0$ and (b) $\sigma < 0$ Ref. 24

and the orientational degrees of freedom must be treated quantum mechanically in order to properly understand the fundamental properties of the solid at low temperatures The molecular centers of mass are only weakly localized with respect to quantum fluctuations because of the relative weak binding forces and the small molecular mass. The rms deviation $\langle u^2\rangle^{\frac{1}{2}}_{H_2} \approx 0.18\ R_0$ where R_0 is the nearest neighbor separation

There are two species of hydrogen molecules One is ortho hydrogen with total nuclear spin $I = 1$ and odd molecular angular momentum J =odd ($J = 1$

at low temperatures). The other species is para hydrogen with total nuclear spin $I = 0$ and even molecular angular momentum $J =$ even ($J = 0$ at low temperatures). There is a strong quadrupole-quadrupole EQQ interaction between ortho-hydrogen molecules in solid hydrogen. The ortho-hydrogen whose molecular axis can have a preferred orientation. Quantum mechanics gives the probability of finding a particular orientation, and shows that the ortho molecule orientational state can be described by the shape of an ellipsoid (Fig. 14) in which the length of a vector from the center to a point on the ellipsoid's surface represents the probability that the ortho molecule is oriented parallel to the vector. At high temperatures there is no preferred orientation, the molecules are disordered as far as their orientations are concerned because of the thermal motion. At low temperatures the orientations will be determined by the configurations that minimize the quadrupole–quadrupole interactions. For two isolated quadrupoles, the minimum energy configuration is a T shape (Fig. 15) in which the quadrupoles are mutually perpendicular.

In contrast to ortho hydrogen, the para hydrogen can be regarded as a symmetric sphere as far as the orientational degrees of freedom are concerned because all the orientations of the para molecular axis are equally probable. At low temperatures three cases can occur:

1. When the concentration of ortho hydrogen $x > 55\%$, the long range orientationally ordered phase will be formed as in Fig. 17 by the strong EQQ interaction.

2. The degree of long range order will be reduced by replacing ortho molecules with spherically symmetric para molecules. When $x < 55\%$ a short range ordered and frustrated phase — A quadrupole orientation glass phase will be observed[15,16] as shown in Fig. 17 and Fig. 18.

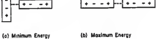

(a) Minimum Energy **(b) Maximum Energy**

Figure 15 Configurations of a pair of interacting axial quadrupoles for (a) minimum and (b) maximum energy

3 At extreme low ortho concentrations for example $x \sim 1\%$ the spherical symmetric para hydrogen will dominate the behavior of solid hydrogen, and the short range order and the frustration effect will be extremely small The low concentration ortho molecules will exist as ortho impurities In this pure para hydrogen region the fast quantum tunneling effect will be obvious In contrast to para hydrogen the motion of ortho molecules is quenched This quenching results from the fact that the ortho molecule is not spherical, it is slightly ellipsoidal and has a small electric quadrupole moment and therefore interacts with other molecules via electrostatic quadrupole quadrupole interactions

$$E_{QQ} = \Gamma(\frac{R_0}{R})^5 F(\Omega_1, \Omega_2) \qquad (27)$$

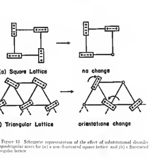

Figure 10 Schematic representation of the effect of substitutional disorder on quadrupolar arrays for (a) a non-frustrated square lattice and (b) a frustrated triangular lattice

F is an angular function which depends on the relative orientations (Ω_1 and Ω_2) of the molecules The strength of the interaction is given by $\Gamma \approx 0.8$K. The available energy levels for a dilute array of the ortho molecules form a band of width $E_Q = 20\Gamma x^{\frac{5}{3}}$ for an ortho concentration x If an ortho molecule is to tunnel then in order to conserve energy the initial and final states can only differ in energy by $\Delta E = hJ_t$ where J_t is the tunneling frequency Of all the available states for an ortho molecule in the band width E_Q of final states, only a very tiny fraction

$$f = \frac{hJ_t}{E_Q} = 2 \times 10^{-7} x^{-\frac{5}{3}} << 1 \text{ for } x > 0.1\% \qquad (28)$$

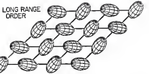

Figure 17 Long range orientational ordering of ortho-hydrogen molecules (Only 2 sublattices of a horizontal plane of the 4 sublattice $Pa3$ structure are shown) Ref 24

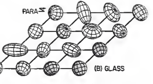

Figure 18 Short range quadrupolar glass ordering at low ortho concentrations The local quadrupolar parameters vary at random from site to site Ref 24

can satisfy the conservation of energy The tunneling of ortho molecules is therefore severely quenched for $x > 0.1\%$ Because we want to test the quantum tunneling model in solid hydrogen we concentrated our interest on pure para hydrogen or very low ortho hydrogen contents

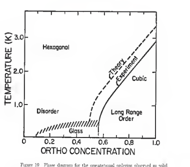

Figure 19. Phase diagram for the orientational ordering observed in solid ortho para hydrogen mixture. The hatched region represents the continuous growth of quadrupolarization on cooling into the glass region. For bulk hydrogen samples, the ortho molecules will convert to para hydrogen at a very slow rate 1.83% per hour.

2.4 Feynman's Ring Exchange[17] Model

The multiple exchange model is consistent with Feynman's ring exchange. Feynman started from the calculation of path integrals in which he noticed that during the particle motion, if the velocity $x_i(u)$ becomes too large, or if the interaction potential V becomes too large, the path gives only a small contribution.

The term $V[x_i(u) - x_j(u)]$ is large when at "time" u particle i and j are close to each other (that is comparable to the hard core radius) and he concluded that the interaction among particles is "kinetic" rather than "potential". He found that the partition function for low temperatures has the form

$$e^{-\beta F} = \frac{1}{N!}\sum_{P}(-1)^{P}\int(\frac{m'}{2\pi\hbar^2\beta})^{3N/2} \times \exp(-\frac{m'}{2\hbar^2\beta})\sum_{i}(\vec{R}_i - P\vec{R}_i)^2$$

$$* \rho(\vec{R}_1, \vec{R}_2, \ldots \vec{R}_n)d^3\vec{R}_1 d^3R_2 \qquad (29)$$

where $P\vec{R}_i$ is the position after permutation. From this partition function we can see that, because of the term $-\exp[\sum_i(\vec{R}_i - P\vec{R}_i)]$, the large distance motion only makes a very small contribution to the total partition function, and it is negligible. We can therefore only consider the nearest neighbor exchange process. Feynman also made a further statement that a permutation among particles can be visualized as a polygon with arrows. The example shown in Fig 11.36 of ref. 17 consists of several cycles of length 1 (particles are not permutated), one cycle of length 2, and two cycles of length 3. Feynman argued again that at low temperatures a side (of a polygon) longer than the average interatomic distance d is not important, thus we may assume that the sides of all polygons that contribute have length of order d (that is the nearest neighbor cyclic permutation!). He mentioned that given a particular configuration $(\vec{R}_1, \vec{R}_2, \ldots \vec{R}_N)$ permutations should be restricted to be such that $\vec{R}_i$ and $P\vec{R}_i$ are close. The conclusion is obvious that the multiple cyclic permutation model is consistent with Feynman's path integral method.

2.5 Three Particle Quantum Tunneling Model in Solid hcp H_2

In the Delrieu and Sullivan model,[12] the observed narrowing of the NMR line shapes of HD impurities in solid para-hydrogen is interpreted in terms of a motional narrowing effect due to quantum tunneling. This model is successful in describing the dependence of the HD line width on the ortho hydrogen concentration and predicts a tunneling frequency $J \sim 1$ KHz. This value can be understood in terms of current views of tunneling in quantum solids which predict that three-body cyclic permutations dominate the tunneling processes in *hcp* ^{3}He and H_2.

In solid para hydrogen (or low ortho concentration) para hydrogen will undergo quantum tunneling in the three particle cyclic permutation model. However, the para hydrogen exchange frequency cannot be observed by NMR experiments because the para hydrogen total nuclear spin $I = 0$. HD molecule is a good candidate to represent the para hydrogen molecule because (1) it has a spherically symmetric wave function, and (2) with proton nuclear spin $I = \frac{1}{2}$ it can be observed by NMR. The exchange motion of HD molecules with nearest neighbor para hydrogen molecules can therefore be investigated by NMR experiments. Low temperature NMR experiments[18,19] on HD (400 ppm) and ortho H_2 (0.1-4 at %) in solid para H_2 have revealed the existence of a significant hitherto unsuspected movement of the molecules in solid *hcp* hydrogen at very low temperatures ($T \geq 25$ mK). The proton NMR line shapes of the HD impurities are apparently Lorentzian and have a temperature independent line width at least five times smaller than that calculated for a rigid lattice. This suggests that the HD line shape is narrowed by some mechanism which modulates the dipole-dipole interactions between the HD molecules and the ortho H_2 molecules. Nevertheless, the linewidths of the signals attributed to isolated ortho H_2 molecules are not narrowed and any mechanism used to explain the motional narrowing of the HD spectra must be effectively quenched [illegible] the ortho H_2 molecules. These properties can be understood in terms of a large three body cyclic permutation rate for molecules in *hcp* hydrogen analogous to that predicted for *hcp* ^{3}He. Delrieu and Sullivan calculated the tunneling frequency by two methods as follows.

1. The first obvious approach is to use the experimental tunneling frequency for solid ^{3}He as a scale to estimate the frequency in solid H_2. As stated earlier, if the three-particle exchange model developed so far has any validity, it should be able to apply to another member of quantum crystals solid para hydrogen beside the solid He. (We consider solid para hydrogen rather than ortho hydrogen to avoid the difficulties associated with the additional degrees of freedom associated with the rotation of ortho molecules. Para molecules have the symmetry of spheres and their tunneling can be treated using the above model.) Since the tunneling rate depends essentially on the available free volume for permuting particles, we expect that the rate for three particle cyclic permutation will be the same in solid para-hydrogen and solid *hcp* ^{3}He when the ratio R_0/a is the same for both solids, where R_0 is the lattice spacing, σ is the characteristic length of the Lennard-Jones potential $[V(\sigma) = 0]$ and $a = 0.8368\sigma$ is the hard-core diameter. See Table V.[11]

Table V. Parameter used in the calculation of the tunneling frequencies in hcp ^{3}He, hcp H$_2$ and hcp D$_2$. R_m and ϵ_m define the minima of the pair potentials of Fig. 1 in reduced units. $a = 0.8368\sigma$ is the hard core diameter (Ref. 20). The compressibilities are taken from the experimental results given in Refs. 12 and 13.

	V_m (cm^3/mol)	R_0(Å)	σ(Å)	a(Å)	R_m	ϵ_m	P (bar)
^{3}He	19.25	3.56	2.556	2.319	1.34	8.32	118
	18.0	3.48	2.556	2.319	1.34	8.32	171
	17.75	3.47	2.556	2.319	1.34	8.32	188
H$_2$ (para)	23.16	3.79	2.96	2.477	1.42	24.95	0
	22.0	3.72	2.96	2.477	1.42	24.95	110
D$_2$ (ortho)	19.95	3.61	2.96	2.477	1.42	24.95	0

	β(10^{-3} bar^{-1})	J (μK)	J (kHz)
^{3}He	1.64	14.4	300
	1.04	1.28	27
	1.00	0.88	18
H$_2$ (para)	0.48	0.46	9.5
	0.36	0.006	0.12
D$_2$ (ortho)	0.23	10^{-6}	$\sim 10^{-5}$

Thus if

$$\frac{R_0(H_2)}{a_{(H_2)}} = \frac{R_0(^3He)}{a_{(^3He)}} \tag{30}$$

then we have

$$\frac{V_m(H_2)}{a^3_{(H_2)}} = \frac{V_m(^3He)}{a^3_{(^3He)}} \tag{31}$$

and we find that corresponding to a molar volume of 22.8 cm^3, the solid ^{3}He is at a density of

$$V_m(^3He) = V_m(H_2)[\frac{a(^3He)}{a(H_2)}]^3 = 15.1 \text{ cm}^3/\text{mol}$$

Kalos *et al.*[20] pointed when $R_{eq} > r_m$ [where r_m is the distance for which $L(r)$ passes through a minimum], i.e. when the zero-point motional energy remains comparable to the potential energy, the wave function for quantum hard core solids is very close to that of a hard sphere quantum solid. In this case the total energy is given by zero-order perturbation theory using the exact wave function of the hard sphere quantum solid. For this reason the wave functions of solid para-hydrogen and solid *hcp* ^{3}He at the same reduced volume are very similar and their tunneling frequencies are therefore of the same order of magnitude in reduced units.[11]

$$J(H_2)\frac{2m_2\sigma_2^2}{\hbar^2} \approx J(^3He)\frac{2m_3\sigma_3^2}{\hbar^2} \tag{32}$$

The experimental values of $J(^3He)$ for *hcp* solid ^{3}He given in Fig. 32 of Ref.[21] is of the order of kHz at density $15 < V_m < 17$ cm^3/mol. This result is at least four orders of magnitude higher than that given by Oyarzun and Van Kranendonk.[22] Testing for tunneling in solid para-hydrogen of the order of kHz provides a sharp test for the multiple exchange model which has been tested only for solid He.

2. The second method of Delrieu and Sullivan is to consider the microscopic physics of tunneling in solid ^{3}He. In order to derive a simple expression fitting the experimental values in *hcp* ^{3}He which is then used to calculate the tunneling frequency in solid H_2. The tunneling frequencies calculated using the model described in section 2.2.2 are in good agreement with those determined experimentally for *hcp* ^{3}He for a wide range of densities. they use the same formula equation (23) to *hcp* H_2 and using the compressibility data published by Wanner and Meyer and find that $J \approx 9$ KHz at $P = 0$ and $J \approx 130$ Hz at $P = 100$ bars. This shows that the tunneling frequency in solid H_2 is also a very sensitive function of the pressure as a result of the rapid decrease of the compressibility

with increasing density. Can HD molecules represent para-hydrogen molecules in solid para hydrogen for an NMR experiment? To answer this question, we need to estimate the cyclic permutation frequency of one HD molecule with two para H_2 molecules. The potential U between the HD molecules and a para H_2 molecule is the same as that between two para H_2 molecules. Nevertheless, the mass of the HD molecules is 3 compared to the mass 2 of the H_2 molecule and this leads to two opposing effects for the effective potential δU in equation 20. The zero point motional deviation of an HD molecule is reduced by a factor of $\sqrt{\frac{2}{3}}$ compared with para hydrogen. The para H_2 molecules surrounding an HD impurity have more available space for their own zero-point motion. The compressibility of the para H_2 around an HD impurity is therefore larger than that of pure para H_2 and δU is therefore expected to decrease slightly. On the other hand, the larger mass of HD is equivalent to an increase in the path length L for the exchange, each displacement being weighted by the mass of the corresponding atom in Schrödinger's equation. The total mass of the exchanging particles (two para H_2 and one HD molecule) is 7 in contrast to the value 6 for pure para H_2. The length L is increased by a factor $\sqrt{\frac{7}{6}}$. The value of $y \propto \delta U\, L^2$ entering in the calculation of the tunneling frequency therefore changes only slightly ($\sim 3\%$) for HD impurities due to the opposing variation of L and δU.

2.6 Observation of Quantum Tunneling in Solid H_2 and the Importance of H_2 Studies

2.6.1 Impurity Motion

In the above analysis, we understood that the multiple exchange model works well for solid He. If this new theory works, it should work for all quantum crystals. Therefore, the observation of quantum tunneling in solid para H_2 becomes a crucial test of the multiple-exchange model. To observe the quantum tunneling frequency, NMR experiments become a powerful and reliable technique.

2.6.2 Vacancy Motion

Besides the impurities in solid para-hydrogen, there exist vacancies, as vacancies exist in any kind of solid. We know that not only point defects, but dislocations and plane defects also exist in any kind of solid. The large zero-point motion determines that the quantum crystals have the property of self annealing, i.e., the line and plane defects can be removed easily from the quantum crystals. The point defects, specially vacancies, will play a major role in the quantum crystals. The density of vacancies is exponentially dependent on the temperature and the density of vacancies X

$$X = n/N = \exp[-\Phi_F/k_B T] \tag{33}$$

when n is the number of vacancies in the N particle system, Φ_F is the formation energy of vacancy. Whereas in the classical solids the defects can be regarded as localized objects which move only occasionally by thermal excitation over intervening potential energy barriers, the defects will become delocalized in the quantum solids, and Andreev[1] has predicted that they will move through the crystal in a coherent manner by quantum tunneling. There are two different kinds of vacancy motions: (a) classical hopping over the potential barriers, and (b) quantum tunneling through potential barriers. To observe the existence of the two different vacancy motions in solid para-hydrogen is another objective of the NMR studies.

2.6.3 Pressure Dependence of Tunneling Frequency in Solid Para-hydrogen

The multiple exchange model predicts a large pressure dependence in quantum crystals.

The observation of the pressure dependence of the HD impurity tunneling frequency will be a severe test for the multiple exchange theory, and such an observation will also provide more information to improve the new cyclic permutation theory in detail.

CHAPTER 3

NUCLEAR SPIN RELAXATION IN THE PRESENCE OF TUNNELING

3.1 Overview of the Relaxation of HD Impurities in Solid H_2

The idea of NMR observations of tunneling in solid H_2 was discussed by Sullivan and Delrieu.[11,24]

The first hint of a hitherto unsuspected motion in solid H_2 came a couple of years earlier than the introduction of the multiple exchange model. Horst Meyer and his students[18] at Duke observed an unexpectedly narrow NMR absorption linewidth associated with HD impurities (400 PPM concentration) in solid para hydrogen (with ortho concentration in the range 0.5–3%).

The HD NMR linewidths were observed to be five time magnitude smaller than the calculated rigid lattice values, while the line shapes attributed to isolated ortho H_2 molecules apparently had their full rigid lattice width. (The para H_2 molecules with $I = 0$ have no nuclear magnetism.) The HD line shapes were Lorentzian to a very good approximation. Delrieu and Sullivan[24] interpreted the narrow HD line shapes in terms of exchange motion, the HD impurities behaving as partners to para H_2 molecules in multiple exchange processes. The HD molecules, carrying nuclear magnetic moments, serve as "tagged" balls to follow the exchange motion of para hydrogen. As the successive 3 body exchanges occur, the HD molecules diffuse through the lattice rapidly in a coherent manner. The magnetic interactions between the HD impurities and the ortho–H_2 molecules is modulated by the motion, and the time average of the interactions responsible for the NMR linewidth is reduced with respect to the rigid lattice value. This is an example of motional narrowing of the NMR line shapes due to the quantum tunneling of the impurities. The motion of the ortho-H_2 molecules is quenched because of the energy conservation law as we discussed in the section 2.3. This can explain why the NMR spectrum of the isolated ortho molecules is not motionally narrowed even through the HD spectrum can be.

To interpret the NMR data we need to formulate the quantum tunneling of the HD molecules through the lattice and their collisions with the ortho-H_2 molecules. As a result of the tunneling, the HD molecules are delocalized and migrate through the crystal by repeated cyclic permutations. The good quantum number in this case is the wave vector $\vec{k}$ rather than the position $\vec{R}(t)$. The energy dispersion is given by

$$E(\vec{k}) = \hbar J_t \sum_{k} e^{i\vec{k}\cdot\vec{R}_0} \tag{34}$$

where J_t is the tunneling frequency. The group velocity for the motion is $V_g = |\frac{\partial E}{\partial k}| = ZR_0J_t$ where R_0 is the lattice spacing and Z is the co-ordination number.

The HD impurities will diffuse through the lattice until scattered by lattice imperfections. The principal source of imperfections will be the elastic strain field surrounding the "static" ortho molecules. The strain field (at long distances) is assumed to be of the form

$$U_{strain}(\vec{R}) = U_0(R_0/R)^n \tag{35}$$

where $n \simeq 6$ for classical strain fields. U_0 is approximately 10 mk. The distance of closest approach will be $R_c \simeq R_0(U_{strain}/\hbar J)^{1/n}$. There are two different regimes: one is the low ortho concentration regime, i.e., gas-like regime, the other is the high ortho concentration regime, i.e., dense fluid regime.

3.1.1 Gas Like Regime

For the gas like regime the ortho concentration is low and the mean ortho separations $R = x^{-1/3}R_0 >> R_c$ where x is the concentration of ortho-H_2 the HD molecules behave as a gas and we can apply ordinary kinetic theory. We have the mean free path

$$\lambda = \frac{1}{n\sigma} \tag{36}$$

where $\sigma = \pi R_c^2$ is the collision cross-section and

$$n = \frac{1}{|\vec{R}|^3} = \frac{x}{a_0^3} \tag{37}$$

then

$$\lambda = \frac{a_0^3}{\pi R_c^2 x} \tag{38}$$

using a random walk model we find that the mean square displacement

$$<< l^2 >> = N\lambda^2 = (\frac{t}{\lambda/v})\lambda^2 = \lambda V_g t \tag{39}$$

where $N = \frac{t}{\lambda/v}$ is the number of steps in time t. And because

$$< l^2 >> = D_g t \tag{40}$$

we have the diffusion constant D_g in the gas like regime

$$D_g = \lambda V_g \tag{41}$$

and

$$V_g = Z R_0 J_1 \tag{42}$$

Finally,

$$D_g = \frac{Z a_0^4}{\pi R_c^2 x} J_1 \tag{43}$$

This is valid for ortho concentrations $x < (J_1/V_0)^{\frac{3}{n}} \sim 1\%$

3.1.2 Dense Fluid Regime

For higher ortho concentrations the HD molecules interact continuously with the elastic deformation field. The motion is still diffusive but now appropriate to that of a dense fluid. As the ortho concentration

$$X > \left(\frac{J_t}{U_0}\right)^{3/n} \sim 1\% \tag{44}$$

the HD molecules will feel strong continuous interactions with elastic deformations such as ortho-H_2 in solid para hydrogen and therefore the behaviors of the HD impurities is that of a dense fluid. The changing rate of momentum

$$\frac{d\vec{P}}{dt} = \nabla U \tag{45}$$

where

$$U = U_0\left(\frac{R_0}{R}\right)^n \tag{46}$$

in the strain field.

The characteristic energy

$$E_{char} = h\Omega_{char} \tag{47}$$

where Ω_{char} is the characteristic frequency. The characteristic time τ_{char} is the time that an HD molecule needs to change its trajectory by a distance R_0, the atomic spacing. Therefore

$$\tau_{char} = \frac{h}{|R_0 \nabla U|} \tag{48}$$

and the diffusion constant

$$D_{dense} \propto \int V_0 V(t)dt \tag{49}$$

and one finds that

$$D_{dense} = V_g^2 \tau_{char} \tag{50}$$

and

$$D_{dense} = \frac{z^2 R_0^2}{n} \left(\frac{J_t^2}{U_0}\right) X^{-(n+1)/3}$$

The quantum diffusion of the HD impurities in the gas-like "impuriton"[25] regime and the dense fluid regime can be followed by NMR studies of the transverse nuclear spin relaxation time T_2, or the linewidth of the continuous wave (CW) absorption spectrum. The transverse relaxation time can be determined from the free induction decay (following a 90° RF pulse)

$$F(t) = \langle I_x(t) I_x(0) \rangle / \langle I_x^2 \rangle \tag{51}$$

which can be simply related to the dephasing $\delta\phi$ of the ^{1}H spins of the HD molecules during "collisions" with the ortho-H_2 molecules

$$F(t) = \langle \exp -i(\sum_{coll} \delta\phi) \rangle = \exp(\frac{1}{2} n \langle \delta\phi^2 \rangle) \tag{52}$$

where $n = t/\tau_c$ is the number of collisions in time t. $\tau_c = D/V_g^2$ is the time between collisions. The relaxation is exponential $F(t) = e^{-t/T_2}$ with

$$\frac{1}{T_2} = \frac{\gamma^4 \hbar^2}{2 R_c^4} \frac{1}{D_g} \sim \frac{\lambda}{J_t} \tag{53}$$

for the impuriton gas regime and

$$\frac{1}{T_2} = \frac{\gamma^4 \hbar^2}{R_0^4} \frac{1}{D_d} \sim x^{(n+1)/3} \frac{U_0}{J_t^2} \tag{54}$$

for the dense fluid regime.

Similarly, the transverse relaxation time T_2 can also be determined by $90_x \tau 180_y$ pulse sequence. The echo height will be

$$S(2\tau) = S(0) e^{-\frac{2\tau}{T_2}} \tag{55}$$

where τ is the time between two pulses.

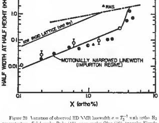

Figure 20 Variation of observed HD NMR linewidth $\sigma = T_2^{-1}$ with ortho H_2 concentration. Solid circles Duke (18) open circles Ohio (19) triangles Florida (46)

The CW lineshape is the Fourier transform of the FID and we expect Lorentzian line shapes with half width at half maximum given by $\delta = \frac{1}{T_2}$ The experimental results obtained in different laboratories are compared with the theoretical predictions in Figure 20

The observed width δ is linear in ortho concentration for $x < 2.5\%$ and a factor of approximately 8 smaller than the calculated rigid lattice value[11] A cross-over to fluid-like regime consistent with the relaxation given by equation

(54) with $n \approx 2.5\%$. The tunneling frequency J_l can be estimated from the experimental data by casting equation (53) in the form

$$\frac{1}{T_2} = \frac{5\pi}{27Z}\frac{X M_{20} X_c^{-\frac{2}{3}}}{J_l} \tag{56}$$

where M_{20} is the second moment for pure ortho hydrogen and $X_c = (J_l/U_0)^{3/n}$ is the concentration for the cross-over between the two regimes. Using $X_c = 2.5\%$ and the linear concentration dependence of T_2 in the impuriton regime, J_l is found to be of the order of 1 KHz at $P = 0$. The calculated value of the HD molecule tunneling frequency is only reliable to an order of magnitude.

3.2 Vacancy-Induced Nuclear Spin Lattice Relaxation in Solid H$_2$

The vacancies in solid helium are believed to travel coherently as vacancy waves at low temperatures rather than hopping randomly as classical point defects. Ebner and Sung[27] have calculated the ground state energy of a vacancy in solid H$_2$. What is particularly interesting for H$_2$ is that there are two bound states for the particle–vacancy interaction potential at $E_1 = 34.1$ K and $E_2 = 95.4$ K (at $P = 0$). The energy barrier to classical particle-vacancy exchange (Fig. 21) is $V_B = 85$ K. Ebner and Sung have also calculated the tunneling energies for both states and find $J_1 = 3.1 \times 10^9$ HZ (0.150K) and $J_2 = 1.1 \times 10^{11}$ Hz (5.14 K).

Using Fermi's golden rule, one can calculate the transition probability[28] for a vacancy tunneling from lattice site $\vec{R}_j$ to site $\vec{R}_l$ where the local crystal fields (for particle displacement) are Δ_j and Δ_l respectively. The rate per unit time is

$$W_{jl} = 2\pi\omega_t^2\delta(\Delta_j - \Delta_l) \tag{57}$$

where ω_t is the microscopic tunneling frequency of vacancies. The diffusion constant for the vacancy motion can be calculated assuming the random walk formula

$$D = \frac{1}{6}\sum_j R_{jl}^2 W_{jl} \tag{58a}$$

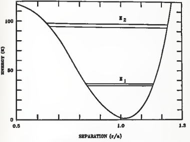

Figure 21 Vacancy molecule interaction potential for solid H_2 (after Ebner and Sung Ref 27) E_1 and E_2 are the two bound states 34 1 K and 95 4 K respectively each level is shown as a doublet, corresponding to the tunneling $J_1 = 0.15$ K and $J_2 = 5.1$ K, respectively

$$D = \frac{1}{6} a_0^2 f X_1 \sum_n W_n P_n \qquad (58b)$$

where a_0 is the nearest neighbor lattice spacing f is a correlation factor (of order unity) which specifies the extent to which the jumps are not random $X_1 = \exp[-(F_v/K_B T)]$ is the vacancy concentration or probability that a given site is vacant (F_v being the vacancy free energy) W_n is the jumping rate from energy level $n(= 1$ or $2)$ of Fig. 17. P_n is the probability that level n is occupied and $R_{jl} = |R_j - R_l|$. For quantum mechanical tunneling through the energy barrier $W_n = J_n/\pi$ (assuming $\Delta_j = \Delta_l$) and for classical thermal activation over the energy barrier V_B, $W_{therm} = (V_B/ma_0^2)^{\frac{1}{2}}$. The self-diffusion rate for vacancy particle motion, considering all processes, is

$$D = \frac{1}{6}a_0^2\{\sum_n (J_n/\pi)P_n + (V_0/ma_0^2)^{\frac{1}{2}}e^{-V_B/k_BT}\}e^{-\Phi_F/k_BT} \qquad (59)$$

where Φ_F is the vacancy formation energy. The calculation of Ebner and Sung yields

$$D = 2 \times 10^{-6}\{1 + 34e^{-61/T} + 300e^{-85/T}\}e^{-112/T}\text{cm}^2/\text{sec} \qquad (60)$$

This theoretical expression for the self-diffusion constant is unusual in that there are two well defined temperature ranges: (i) classical hopping by thermal activation at high temperatures with an activation energy $E_A = \Phi_F + V_B = 197K$ for $T > (E_B - E_2)/\ln(W_{class}/J_2) \approx 12K$ and (ii) quantum tunneling at low temperatures with $E_A = \Phi_F = 112K$ for $T < 11K$. It is important to note that although there are three terms in the expression for D (eq. (60)) with different temperature dependences, there are only two temperature regimes because the second term in equation (60) does not dominate for any temperature. The first term dominates the second term for $T < (E_2 - E_1)/\ln(J_2 - J_1) \approx 17K$ (corresponding to $E_A = \Phi_F + E_2 - E_1 \simeq 173K$). One therefore expects to observe only classical hopping with $E_A = 197K$ at high temperatures and expects that the quantum tunneling with $E_A = \Phi_1 = 112K$ can be observed at low temperatures (for example $T \approx 11K$). The self-diffusion constants can be determined from the measurement of the nuclear spin–lattice relaxation time T_1. NMR is sensitive to the presence of vacancies through their diffusive motion. As the vacancies migrate through the lattice by exchange with atoms or molecules, the intermolecular nuclear spin–spin interactions become time-dependent because of the molecular motion. The spectral components of the motion at the nuclear Larmor frequency ω_L and at $2\omega_L$ determine the nuclear spin–lattice relaxation induced by the vacancy motion. The relation between the microscopic vacancy tunneling frequency ω_V and the characteristic frequencies that determine the modulation of the nuclear spin–spin interactions need to be established with care.[29,30] If in a given crystalline structure, a vacancy can migrate from a given lattice site to a neighboring site with a characteristic frequency ω_{m0}, the time-dependent jump frequency for a given molecule is

$$\omega_m(T) = X_V(T)\omega_{m0} \tag{61}$$

where $X_V(T)$ is the number of vacancies in thermal equilibrium at temperature T. ω_{m0} is related simply to the tunneling frequency ω_t by a numerical constant which depends on the lattice structure. Moment calculations[29] show that for tunneling involving only nearest neighbors

$$\omega_{m0} = A\omega_t \tag{62}$$

with $A = Z\sqrt{2\pi/15}$ for coordination number Z.

The intermolecular dipole–dipole interaction between two molecules are modulated at a rate

$$\omega_D = 2\omega_{m0} = 2AX_V(T)\omega_t \tag{63}$$

NMR experiments can therefore be used to determine the microscopic jump frequency ω_t and the formation energy and barrier energy through the absolute values and the temperature dependence of the relaxation times, respectively. The nuclear magnetic relaxation can be described in terms of an energy bath model consisting of several energy reservoirs: the nuclear Zeeman energy (Z), the vacancy (V), the tunneling excitations (E), the phonons (P) and the thermal bath (or walls) (B). If the Zeeman energy is perturbed, thermal equilibrium is restored by transitions between the nuclear Zeeman energy levels induced by the fluctuations of the dipole–dipole interactions. If the dipolar interactions are expressed in terms of irreducible tensorial operators $T_{\ell m}$ (which transforms analogously to the spherical harmonics $Y_{\ell m}$) the relaxation rate (for a polycrystalline sample) is given by

$$\frac{1}{T_1} = \frac{2}{3} M_2 \sum_{m=1,2} m^2 J_{lm}(m\omega_L) \tag{64}$$

where M_2 is the Van Vleck second moment for the dipole–dipole interactions and the $J_{lm}(m\omega_L)$ are the spectral densities of the spin–spin correlation functions $\langle T_{lm}(t) T^{+}_{lm}(0) \rangle$ at the nuclear Larmor frequency ω_L. The $J_{lm}(m\omega_L)$ are difficult to evaluate directly from the microscopic motion and are often approximated by Lorentzian functions

$$J_{21}(\omega_L) = \omega_D^{-1} / [1 + (\omega_L/\omega_D)^2] \tag{65}$$

At very low temperatures the number of vacancies is too small to provide an effective interaction and this vacancy induced relaxation mechanism becomes "frozen out" and other processes take over. In solid H_2 we must consider the two distinct molecular species.

There is a competing mechanism for the relaxation of ortho H_2 resulting from the modulation of the intramolecular dipole–dipole interaction of each molecule by rapid molecular reorientations. The latter is determined by the electric quadrupole–quadrupole (EQQ) interactions between ortho molecules and it overwhelms the vacancy-induced mechanism for temperatures close to the melting point where the number of vacancies is high. Weinhaus and Meyer[31] observed vacancy induced relaxation for $10.5 < T < 13.5$K for relatively high ortho concentrations and observed a variation in T_1 by a factor of 5. Bloom[33] saw only the E_{QQ} mechanism for solid H_2, but did observe vacancy effects for solid HD.

In order to test for the possible quantum tunneling of vacancies in solid H_2 we needed to observe vacancy relaxation at temperatures significantly lower than those previously studied. We therefore chose to study samples containing low ortho concentrations $(0.5 - 2.5\%)$ and prepared with small concentrations of HD impurities (typically 1%). (The natural HD abundance is 0.04%.) The ortho H_2 molecules relax very rapidly via the EQQ mechanism with $T_{1Q} = 1.78(\Gamma/K_B)X^{\frac{5}{3}}$ for these ortho concentrations and at high temperatures.[34] The direct relaxation of the HD molecules to the lattice is, however, very slow and one observes an indirect relaxation mediated by the spin–spin coupling between the HD molecules and the ortho-H_2 molecules. The cross relaxation can be analyzed by treating the ortho-H_2 spins and the proton spins of the HD molecule as two weakly coupled energy reservoirs a and b respectively (Fig. 22).[33]

The coupled rate equations for the inverse nuclear spin temperature λ^a and λ^b of the two energy baths is given by[33,35]

$$\frac{d\lambda^a}{dt} + [\frac{1}{T_1^{aa}} + \frac{1}{(T_x^{ab})_1} + \frac{1}{(T_x^{ab})_2} + \frac{1}{(T_x^{ab})_0}](\lambda^a - \delta^a)$$

$$= [\frac{1}{(T_x^{ab})_0} - \frac{1}{(T_x^{ab})_2}](\lambda^b - \delta^b) \qquad (66a)$$

$$\frac{d\lambda^b}{dt} + [\frac{1}{T_1^{bb}} + \frac{1}{(T_x^{ba})_2} + \frac{1}{(T_x^{ba})_2} + \frac{1}{(T_x^{ba})_0}](\lambda^b - \delta^b)$$

$$= [\frac{1}{(T_x^{ba})_0} - \frac{1}{(T_x^{ba})_2}](\lambda^a - \delta^a) \qquad (66b)$$

$\lambda^{a(b)} = \gamma_{a(b)}\hbar B/k_B T_s^{a(b)}$ and $\delta^{a(b)} = \gamma_{a(b)}\hbar B/k_B T_L$ where $\gamma_{a(b)}$ are the nuclear gyromagnetic ratios, B the applied magnetic field, and $T_s^{a(b)}$ and T_L are the

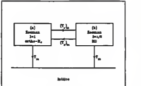

Figure 22 Schematic representation of the coupling and relaxation of the two nuclear spin energy baths for (a) ortho H_2 and (b) HD molecules.

nuclear spin temperatures and lattice temperature respectively. T_1^{aa} and T_1^{bb} are the relaxation times in the absence of any coupling. The $(T_x^{ab})_m$ represent the cross-relaxation processes given by

$$\frac{1}{(T_x^{ab})_1} = \frac{2}{3} M_2^{ab}(X) J_{21}^{ab}(\omega_a) \tag{67a}$$

$$\frac{1}{(T_x^{ab})_2} = \frac{4}{3} M_2^{ab}(X) J_{22}^{ab}(\omega_a + \omega_b) \tag{67b}$$

$$\frac{1}{(T_x^{ab})_0} = \frac{2}{9} M_2^{ab}(X) J_{20}^{ab}(\omega_a - \omega_b) \tag{67c}$$

$$\frac{1}{T_x^{ba}} = f \frac{1}{T_x^{ab}} \text{with } f = \frac{N_a I_a(I_a+1)}{N_b I_b(I_b+1)}$$

N_a and N_b are the number densities for the a and b spins, respectively. $M_2^{ab}(X)$ is the rigid lattice second moment for the intermolecular dipole-dipole interactions between the a and b spins for an *ortho* concentration X. The J_{lm}^{ab} are the spectral densities for the (lm)-th component of the dipolar interactions, and ω_a and ω_b are the nuclear Larmor frequencies of the a and b spins respectively.

The ortho-H_2 molecules relax rapidly to the lattice via the EQQ mechanism $T_{1Q} \approx 2-4msec$ for X (ortho) ≈ 0.5–2%, and one observes the cross relaxation of the HD molecules (the b spins) to the ortho-H_2 molecules (the a spins). The cross relaxation rate is given by

$$\frac{1}{(T_x^{ba})} = \frac{2}{9} f M_2^{ab}(X) J_{20}(0) \tag{68}$$

with $J_{20}(0) = \omega_D^{-1}(T)$. Because the HD molecules are mobile while the ortho molecules remain fixed $\omega_D = \omega_M(HD)$, in contrast to equation (63). Studies of this cross relaxation allow one to explore the temperature dependence of the vacancy motion over a wider temperature range than possible in previous studies[31–33,36,37]. Determination of the characteristic motional frequencies $\omega_{D(T)}$ also allows one to calculate the self-diffusion constant from the relation $D = \frac{1}{6} a_0^2 \omega_m(T)$.

CHAPTER 4

EXPERIMENTAL APPARATUS

4.1 Cryogenics

A ^{4}He Dewar with a plastic inner wall is used in this experiment. The volume of the Dewar is 40 liters and the evaporation rate is 7.5 liters/day for pulse NMR experiments and 10 liters/day for CW NMR experiments. On one occasion the Epoxy between the Aluminum top flange and the plastic inner wall was broken and caused the evaporation rate to increase to 40 liters/day. After repairing at the factory, the Dewar is working at normal conditions and is monitored by the Helium gas flow meter. A continuous superconducting wire[38] He level detector and two diode level detectors are also used to measure the level of liquid helium to safeguard the normal working condition of the cryogenics and the superconducting magnet (See Figure 23.)

A dilution refrigerator is used for the low temperature data taking. The working principle is that the temperature will decrease by pumping ^{3}He from the ^{3}He rich phase in the mixture of ^{3}He and ^{4}He by dissolution into the ^{3}He dilute phase.[39] Because of the large heat release caused by the conversion from ortho-H_2 to para-H_2, our H_2 sample cell cannot be cooled below 37 mK, although the limit without an H_2 sample is specified below 4 mK (according to manufacturer SHE). The temperature was monitored by a calibrated carbon glass thermometer[40] attached to the copper cold finger of the NMR cell. The temperatures were also checked using the total NMR absorption signal and the FID height of the pulse NMR as a measure of the mean temperature of the hydrogen

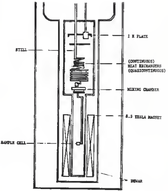

Figure 23 Diagram of cryogenics

sample. The temperature regulator is connected with the heaters of the mixer and still of the dilution refrigerator to adjust and stabilize the temperature.[45] The NMR method was very reliable at low temperatures, but was unreliable near the melting point because a portion of the sample tended to migrate up the fill line and we relied on the carbon glass thermometer to determine the temperature in this region.

4.2 NMR Sample Cell

The NMR cell consisted of a kel-F sample chamber (3mm I.D. 3mm length) (see Fig. 24).

Both ends of the cell were sealed by a cylindrical copper end caps which were carefully machined to a diameter slightly larger than that of the kel-F chamber (the diameter was very carefully calculated to accomodate the thermal dilatation) and a seal reliable to 150 bar was obtained by the thermal contraction of the kel-F following initial warming to 150deg C during assembly. One of the end caps formed an integral part of a thermally regulated cold finger of OFHC copper while the other was fed by the hydrogen fill line. Thermal contact to the sample was assured by a brush of very fine copper wires (0.001mm O.D.) which were soft soldered to the cold finger.

4.3 Pulsed NMR Apparatus

The radio frequency coil wound around the sample chamber was connected to an RF pulse duplexer (at room temperature) by a homemade cryogenic cable (stainless steel outer conductor, teflon dielectric and nominally 50Ω) cut to $\frac{3\lambda}{2}$. The duplexer was a "Lumped-circuit" designed to optimize the matching of the RF power pulse to the NMR circuit while protecting the receiver. The output

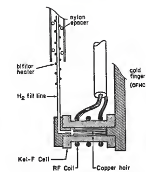

Figure 24. Schematic drawing of the NMR cell. The coil former is machined from Kel-F and forms a heat-shrink fit over the copper end caps.

of the duplexer was amplified by a three-stage, low-noise, narrow-band UHF amplifier employing dual-channel MOSFET transistors.[42]

The gain of the RF amplifier was observed to be temperature dependent, and to ensure long term stability for the calibration of the overall gain, we had to regulate the temperature of the amplifier. This was achieved by putting the amplifier inside a thermally insulated chamber and regulating its temperature to ±0.1°C. The output of the amplifier was detected coherently using a doubly-balanced mixer where the local oscillator source was derived from the RF generator which fed the gates of the RF pulse system. An adjustable coaxial line was used to obtain the correct phase of the source at the mixer. After coherent detection automatic signal averaging techniques were used to record the free-induction decays following each pulse. A diagram of the pulse NMR apparatus is sketched in Figure 25.

Four output switches of the gate box lead to four different gates which allows one to change the phase by 0°, 90°, 180°, and 270°, respectively. The frequency of the pulse NMR is operating at 268 MHz which corresponds to a magnetic field $H_0 = 6.3$ Tesla. The magnetic field is provided by a superconducting magnet which can supply the magnetic field as high as 9 Tesla at 2 K. The large diameter and long coils of the magnet and the small size of the sample cell safeguard the stability and the homogeneity of the magnetic field at the region where the hydrogen sample is located. The advantages of the high frequency (high magnetic field) are (1) the high resolution, high sensitivity which is characterized by the ratio of signal to noise S/N, and (2) the short dead time which is proportional to the reciprocal of the frequency.

4.4 Continuous Wave (CW) NMR Apparatus

The continuous wave NMR apparatus is described in Figure 26.

Instead of the use of a duplexer in pulse NMR which we discussed above, a hybrid T(43) is used to fulfill the purpose of transferring only the sample response to the receiver. The hybrid -T is similar to the magic T at high frequencies which was invented in 1973.[43] The RF input is split to two arms: (1) a dummy

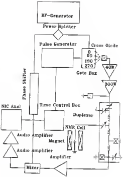

Figure 25 Diagram of the pulse NMR apparatus

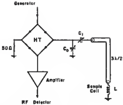

Figure 26 Diagrammatic representation of the NMR bridge circuit employing a quadrature hybrid tee (HT) for continuous wave NMR Capacitors C_0 and C_1 match the coil impedance to the 50Ω input port of the tee

load and (2) the NMR circuits which are both matched to 50Ω We were very careful to test the impedance of the NMR circuit at the value of 50Ω at the frequency 268 MHz without H_2 sample to safeguard the matching condition of the NMR circuit and the dummy load If the resonance frequency (268 MHz) was not satisfied, we do not expect to receive any signal from the output of the hybrid T because of the phase difference 180° in the two branches of the hybrid

T. At resonance the matching of the two branches is broken and only the NMR change will be detected in the receiver. In practice, a small deliberate deviation from ideal phase or amplitude matching is adjusted. The small deviation which is carefully adjusted has the advantage that one obtains (1) an amplification effect and (2) a distinct signal (dispersion or absorption) instead of a mixture. A modulated sweep field is provided by a sweep coil in addition to the static high field (provided by the superconducting magnet). This auxiliary field repeats the up and down procedure to draw the NMR spectra at the resonating frequency and this field is sinusoidally modulating by 200 Hz. A lock in amplifier is used in the CW NMR experiment.

4.5 Precise and Efficient In Situ Ortho-Para Hydrogen Converter[44]

We needed samples of hydrogen with accurately known ortho concentrations in the range 0.1 – 2.5% in order to investigate the diffusion of isotopic impurities (HD) and Ortho-H_2 impurities in solid para hydrogen at very low temperatures using NMR [28,45–48]. In addition, the samples had to be prepared in situ, i.e. in close proximity to the low temperature NMR cells, to avoid the significant back- conversion that occurs in passing the gas through stainless steel tubing at high temperatures or over surfaces exposed to air that cannot be baked out. We tested chromic oxide as a low temperature catalyst. This is available commercially as Oxisorb which consists of silica gel impregnated with CrO_3, the oxide being bonded to the silica structure via hydroxyl groups. This material can absorb very large quantities of oxygen (80% by stoichiometric measure) via the reaction and retains its high efficiency even after a large number of regenerations.

The catalyst was placed in a small (10 cm^3) OFHC copper chamber whose temperature was regulated to a precision of ±5 mK in the 15 – 30 K range

Silicon diode thermometers (type 1N4144) affixed to the copper walls were used to monitor the temperature, one as a sensor for the regulating feedback loop and a second as an independent sensor. The diodes were calibrated against a calibrated carbon glass thermometer.[49] A length of 40 AWG copper wire was used as a weak thermal link to a 4K plate and provided the only cooling. The inlet and outlet H_2 lines were made from thin walled cupronickel capillary and provided with independent heaters.

Normal H_2 (corresponding to ~ 2 layers on the gel) was absorbed onto the converter (with the outlet tube maintained hot (T > 35 K)) and the converter then maintained at a certain temperature T_0 at which temperature the desired concentration of ortho H_2 was obtained. The reaction time t for conversion was less than 10 minutes. To safeguard the accuracy of concentrations of ortho H_2 (e.g. 2.5 ± 0.1 %) we waited 2 hours. The NMR cell at the other end of the outlet tube was then cooled below T_0 and the accumulation of hydrogen in the cell monitored by NMR. The H_2 sample was sent back to the converter by warming the sample cell and cooling the converter cell and kept at T_0 for another 2 hours. After repeating such sequences several times (5—6 times)) the ortho concentration was measured by two methods: (1) the nuclear spin-relaxation time T_2 was measured at 4.2K and compared with the Hardy and Gaines[50] calibration which is used by many as a standard, and (2) the ratio of the ortho-H_2 NMR signal to the HD impurity NMR signal was determined for a known HD concentration. (We prepared samples with 1.1% HD concentrations in order to study the motion of the HD molecules at low temperatures.) In all cases we found that to within the accuracy of the measurements (± 0.1% at X = 2.5% and many different

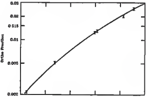

Figure 27 Comparison of the ortho-H_2 concentrations obtained from the in situ ortho-para converter at temperature T with the equilibrium value calculated for free molecules (solid curve). The ortho-H_2 concentrations were determined from comparisons of the HD and ortho-H_2 echo amplitudes at low temperatures and T_2 measurement of pure hydrogen sample data.

concentrations (see Fig. 27) the concentration X was equal to that calculated for the equilibrium value (for independent molecules) at the temperature T_0.

Variations that could be expected because of the differences between the rotational energy levels of the adsorbed molecules and those of the free (vapor phase) molecules were not seen. This is attributed to the fact that the samples used are drawn from the gas phase which is in equilibrium exchange with the adsorbed molecules.

A large number of samples with concentration in the 0.2–3.0% range have been prepared over an 18 month interval without any observed deterioration of the speed of the conversion or any appreciable deviation from the equilibrium value. The whole system had been cycled to 300K four times during this period without any detectable loss of efficiency. From the above discussion, this method has also proved to be the most reliable for producing samples with accurately known ortho concentrations compared with two other methods that we have used: (1) natural conversion (which needs a long period to obtain the low concentration samples)[51,52] and (2) condensing a converted gas (para-hydrogen) into the low temperature sample cell through a tube which is at room temperature.[46]

4.6 Pressure Gauge and Pressure Detector

To observe the pressure dependence of the transverse relaxation time T_2 of the HD impurities in the para-hydrogen the samples were pressurized using ^{4}He. Liquid helium was condensed directly on top of H_2 sample and the pressure read by a pressure gauge (Heise Model 45441 external to the cryostat). The converter pot and the fill line above the pot were heated above 2K to prevent solidification of the ^{4}He for applied pressures $P > 25$bar.

A home made pressure detector (Fig. 24) was mounted directly on the opposite end of the NMR cell (i.e. the H_2 sample is sandwiches by the pressure entrance line and the pressure detector) to verify that the pressure was transmitted to the sample even when the fill line at the entry to the NMR cell contained solid ^{4}He; otherwise the pressure detector will show no response.

4.7 Data Acquisition

A Nicolet fast signal analytical instrument (model LAS 12/70), a chart recorder and a digital PDP 11/74 computer using "C" language and Unix where

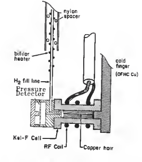

Figure 28 Schematic drawing of the NMR sample chamber The coil former is machined form KEL-F and forms a heat-shrink fit over the copper snouts at both ends and is vacuum tight to 500psi The pressure detector is mounted at high pressure experiment

used to record the signals A program automatically takes measurements of four thermometers distributed at different levels in the cryostat, namely the mixer still, plate heat exchange and the 1 Kelvin pot The Nicolet instrument receives the signal averages the pulse NMR measurements performs Fourier transformation, baseline correction smoothing integration and other mathematical treatments The Nicolet averager analysis instrument has worked satisfactorily after data taking for six years An interface between the Nicolet and the PDP 11 computer provides a data dump and analyses which are stared in the computer Six terminals are used by different members of the group with the computer operating in a multi user mode under the Unix system Recently we set up another IBM 386 in the lab The chart recorder can also take data at the same time that the Nicolet averager is working The CW spectra are always drawn on the chart recorder Several programs were written for data analysis such as spline (draws smooth curves on data points) and best-fit program to minimize the square deviation Two HP plotters and two printers (one is worked with the PDP 11 and another is worked with the IBM 386 PC) A Leroy program is used to draw diagram at the publication quality

CHAPTER 5

EXPERIMENTAL RESULTS AND DISCUSSION

5.1 Sample Preparation

We used 3 different methods to make low ortho concentration para-hydrogen samples. Those methods are the following:

1. Aging from normal H_2 samples at low temperatures, to obtain low ortho H_2. This takes seven months to reach 1% starting with 75%.

2. Condensing a sample from a gas mixture of 1.1% HD and nearly pure para H_2 (ortho $H_2 < 0.1\%$). Significant back conversion occurred during the condensation process (when the gas passed briefly through polyvinyl chloride tubing at room temperature). The ortho concentration of the solid sample was determined from the measurements of the distinct NMR line shapes and NMR echoes of the HD and ortho H_2 signals at low temperatures.

3. Using a converter which was located a short distance from the NMR cell. A gas mixture of 1.1% HD and "normal" H_2 (75% ortho) was first condensed into the ortho-para converter pot containing a chromic oxide gel which was located close to the sample cell. The desired ortho concentration was obtained by regulating the temperature of the converter very accurately and allowing the ortho-hydrogen to convert to the thermal equilibrium value. The converted mixture was then transferred to the NMR cell by lowering the temperature of the cell.

The samples made by the above three methods were carefully annealed at 13.5 K for approximately 6 hours. The final ortho concentration was determined unambiguously by direct comparison of the very distinct NMR echo shapes of the

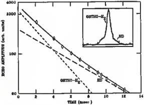

Figure 29 Observed relaxation of the NMR echoes as a function of time at low temperatures ($T = 0.22$ K) The inset shows the distinct HD and ortho-H_2 contributions to the NMR echo with full widths at half height of 1.12 and 0.25 ms respectively The relaxation of the peak echo height (solid line) is analyzed assuming exponential decays for the HD and ortho-H_2 components (broken lines)

HD and the ortho-H_2 signals at temperatures below 1K (see inset to Fig 29) which is consistent with the two distinguishable CW NMR line shapes (Fig. 30)

Two distinguishable relaxation times, $T_{2\,ortho}$ and $T_{2\,HD}$ (Fig 29) can be used to double check the concentration of ortho-H_2 At low temperatures the ^1H relaxation of the HD molecules can be easily distinguished from that of the ortho-H_2 by identifying the different contributions to the echo A decomposition of the peak amplitude of the echo assuming two distinct exponential decays (Fig

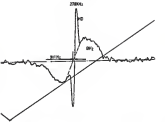

Figure 30 Original CW NMR data taken at 268 MHz Two distinguishable CW NMR absorption line shapes the narrow line is corresponding to the 1 1% HD molecule the broad line is corresponding to the isolated ortho H_2. The pairing ortho-H_2 lines are ±43 KHz away from the center which is not shown on this diagram.

29) was found to provide an accurate description for all the echo decays observed at low temperatures

5 2 Pulse NMR Sequence

The nuclear spin spin relaxation time T_2 measurements were carried out using a phase- coherent pulse system operating at 268 MHz RF pulse sequences of $\frac{\pi}{2} - \tau - \pi$ were used to determine T_2 The nuclear spin-lattice relaxation time T_1

measurements were carried out by $\frac{\pi}{2} - \tau - \frac{\pi}{2}$ RF pulse sequences and $\pi - \tau - \frac{\pi}{2}$ RF pulse sequences

Narrow (8–10 μsecond) high power RF pulses were used to cover the complete NMR spectrum of both the HD impurity molecules and the ortho-H_2 molecules. The amplitude of the RF magnetic field in the rotating frame was 12 gauss. Washburn *et al.*,[53,54] used very long RF pulses (100–150 μsec.) in order to saturate only the relatively narrow HD component of the spectrum, but the interpretation of the relaxation is difficult for the long low-power pulses.[55] To avoid this difficulty, we worked in the short pulse limit (8–10 μsec.) for which the relaxation times T_1 and T_2 are very reliable.

5.3 Temperature Dependence of T_2.[46]

Narrow (8–10 μs covering $\sim$ 25 KHz)RF pulses were used to cover the complete spectrum of the HD molecules and the isolated ortho-H_2 molecules (but not the pairs). The values of T_2 obtained for the sample before melting and for the sample after melting and recondensation show very little variation.

Three distinct temperature regimes are observed. (1) At low temperatures, $0.1 < T < 6.5K$, T_2 is essentially independent of temperature and significantly longer than the rigid lattice value. (2) at intermediate temperature $6.5 < T < 9.5K$, T_2 decreases to a minimum of 0.94 $msec$ at $T \approx 8.2K$, and (3) above 9.5K, T_2 increases exponentially with temperature until the sample melts. The low-temperature behavior (Fig. 31) is attributed to quantum tunneling of the HD molecules which diffuse as a dilute gas scattering from the weak elastic strain fields surrounding the quasistatic ortho-H_2 molecules.[45]

Our results are consistent with the measurements of Meyer and coworkers[53,54] for HD concentrations equal to the natural abundance. The low temperature values of $T_2 = 3.2 msec$ (at 100 mK) were obtained after waiting

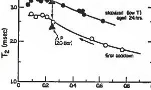

Figure 31. Temperature dependence of the ^{1}H nuclear transverse relaxation times of the HD molecules at low temperatures where the ortho-H_2 (2.1%) and HD (1.1%) components can be distinguished (see Fig. 29.30). The lower curve gives the result for the initial cool down and the upper curve after waiting 24 hours to allow for the clustering of ortho molecules into pairs. The broken line is the estimated rigid lattice value.

for completion of the clustering of ortho molecules into pairs (see Fig. 31). This clustering increases the value of T_2 because the ortho-H_2 pair spectra extends out to ±43 kHz well beyond the HD spectrum and mutual spin flip-flops ($I_1^+ I_2^-$) are forbidden by energy conservation. The difference in T_2 before and after clustering (2.7 and 3.2 *msec* respectively) can be accounted for quantitatively.

The observed values of T_2 (before clustering) are a factor of 7 larger than the value (0.35 *msec*) estimated for a rigid lattice[53,54] and a factor of 5.4 larger than those values measured at high temperatures by Buzerak, Chan and Meyer[56] for an "equivalent" sample containing only ortho-H_2 impurities. We consider a 2.5%

ortho content to be "equivalent" to a 2.1% ortho ($I = 1$) plus 1.1% HD ($I = \frac{1}{2}$) mixture for a rigid lattice. This is because of

$$2.1\% \times I_{oH_2}(I_{oH_2}+1) + 1.1\% \times I_{HD}(I_{HD}+1) = 2.5\% \times I_{oH_2}(I_{oH_2}+1) \quad (69)$$

1. At low temperatures $T < 6.5$K. We have remeasured T_2 for a 2.5% ortho H_2 sample (without adding HD) using the method described here and find values in excellent agreement with Buzerak, Chan and Meyer (Fig. 28) and consider this to be a reliable measure of the rigid lattice value.

This very large effect on T_2 obtained by simply replacing part of the ortho H_2 by HD can only be understood if the HD impurities are mobile. Comparing the prediction of a tunneling frequency ~ 1 kHz by Delrieu and Sullivan, we find an experimental value of the tunneling frequency $J_t = 1.54 \pm 0.08$ kHz for the HD molecules.

2. In the intermediate temperature regime, only a single relaxation is seen for both the HD and ortho H_2 components. T_2 passes through a minimum of 0.94msec. This line- broadening effect on warming indicates an effective breakup of the coherent motion of the HD molecules at these temperatures. This interference can be caused by scattering with phonons[57–59] (or with vacancies) and has been seen very clearly for ^{3}He impurities in solid ^{4}He by Allen and Richards.[2,3] Landesman[57] has shown that for the phonon process

$$D_{scatt} = \frac{1}{3} Z J_t^2 a^2 \tau_{IP} \quad (70)$$

where Z is the coordination number and the impurity-phonon scattering frequency

$$\tau_{IP}^{-1} = A(J/s)^2(\theta_D/T)^9 \times \Omega_D^{-1} \quad (71)$$

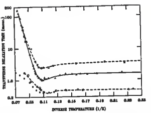

Figure 32. Temperature dependence of the ^{1}H nuclear transverse relaxation time of the HD molecules. The solid line is a fit to the data using phonon impurity scattering to describe the minimum and classical vacancy motion to describe the high-temperature behavior. The triangles represent a sample of 1.1% HD and 2.1% ortho H_2 and the circles represent a 2.5% ortho H_2 sample (stars represent 2.4% ortho H_2). The squares represent a sample of 1.1% HD and 0.5% ortho-H_2. Ref 56

θ_D is the Debye temperature, Ω_D is the Debye frequency and s is a coupling constant (estimated to be $\frac{1}{3}$ for ^{3}He impurities in ^{4}He and $\frac{1}{2}$ for HD in solid H_2). Landesman finds $A = 2.2 \times 10^{-4}$ but there is considerable variation in the calculations.[57–59]

Our test fits for this T^9 phonon scattering and for vacancy scattering are identical which is shown by the solid line in Fig. 27 (with $A = 4.5 \times 10^{-3}$ in the phonon scattering case). The existence of the minimum is further evidence for the existence of the quantum tunneling at low temperatures. The low temperature value of T_2 can not be attributed to rigid lattice values. A minimum has also been observed for the nuclear spin lattice relaxation time in the same temperature range. Broadening on warming for motionally narrowed systems has also been seen in electron-spin-resonance studies of color centers at very low temperatures. To identify the existence of the minimum of T_2 of the H impurities, we repeated the warming up and cooling-down procedure several times. We melted the sample and recondensed it to test the reproducibility of the measurements of T_2. We made different ortho concentration with 1.1% HD samples. The existence of the minimum of T_2 of the HD impurities was proved without exception.

3. In the high temperature regime, a new motional process becomes effective because the concentration of vacancies $X_1 = \exp(-E_1/k_BT)$ becomes non negligible. We have been able to fit the temperature dependence over the entire range studied using the phonon– impurity scattering rate given above and a classical self-diffusion for vacancies given by

$$D_{vac}^{class} = 5.7 \times 10^{-3} e^{-(E_B+E_1)/k_BT} \mathrm{cm}^2\mathrm{sec}^{-1} \tag{72}$$

where the activation energy $E_B + E_1 = 196.8 \pm 1.4$ K. This is the first reported measurement of the vacancy diffusion for solid para hydrogen (very low ortho concentration). Earlier work was limited to ortho para mixtures for $0.16 < x < 0.70^{(31-34)}$ (Table III Ref. 31).

The vacancy tunneling process with

$$D_{vac}^{tv} = D_0^{tv} \exp(-E_1/k_BT) \tag{73}$$

cannot be excluded as it gives an overall fit almost identical to that obtained using the phonon process for $D_0^{qu} = 1.9 \times 10^{-8}$ cm^{2}sec^{-1} and $E_t = 91 \pm 10$ K which are to be compared with Ebner and Sung's values of 2×10^{-6} cm^{2}sec^{-1} and 112K, respectively. It should be noted that for these values for the vacancy tunneling, the crossover from the classical to the quantum regime would not have been seen in earlier experiments. The low temperature side of the minimum cannot be described by the parameters for classical vacancy diffusion determined from the high temperature measurements. The values for $E_B + E_t$ and D_0^{class} for the best overall fits vary a little according to whether the minimum is interpreted as a phonon or as a vacancy scattering mechanism (Table VI).

Table VI. Parameters used in description of temperature dependence of T_2

Scattering mechanism	Vacancy motion	$E_B + E_t$ (K)	E_t (K))	D_0^{class} (cm^2/sec)	D_0^{qu} (cm^2/sec)
Phonons	classical	197 ± 2		5.7×10^{-3}	
Vacancies	classical and quantum[a]	193 ± 2	91 ± 10	5.1×10^{-3}	1.9×10^{-8} [b]
	Ebner and Sung[c]	197	112	6×10^{-4}	2×10^{-6}

[a] $D_{total} = (D_0^{qu} + D_0^{class} e^{-E_B/k_BT}) e^{-E_t/k_BT}$

[b] Assuming a vacancy-impurity scattering cross section $\sigma = 1$ in units of a_0^2

[c] Reference 27

5.4 Temperature Dependence of T_1

The spin-lattice relaxation measurements were carried out using a phase coherent pulse system operating at 270 MHz. $90° - t - 90°$ RF pulse sequences were used to determine the T_1 with RF fields amplitudes of approximately 10 gauss.

The relaxation was observed to consist of a small short time contribution ($t < 2msec$), which we attribute to the ortho-H_2 relaxation, and a long time component which we interpret as the cross coupling relaxation T_x between the HD molecules and the ortho- H_2 molecules. Fig. 33 shows the temperature dependence of the long-time relaxation. Three distinct temperature regimes are observed.

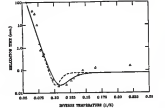

Figure 33. Temperature dependence of the observed nuclear spin lattice relaxation of HD impurities (1.1%) in solid H_2 (1.8 -2.1% ortho). The solid line is calculated for a vacancy-induced relaxation if quantum tunneling is included and the broken line is the contribution for classical tunneling alone. The observed relaxation is attributed to cross relaxation between the HD impurities and the ortho-H_2 molecules.

1. at low temperatures, $1.5 < T < 7\mathrm{K}$, T_1 has only a weak approximately linear temperature dependence;

2. at intermediate temperatures $7 < T < 11\mathrm{K}$, T_1 passes through a minimum and

3. above 11 K, T_1 increases exponentially with temperature until the sample melts.

These results appear similar to those observed for the spin echo decay in the same sample and similar samples[46] but with the important difference that the temperature effects of T_1 are more dramatic. T_1 varies by ~ 5000 in the high temperature regime (T_2 varies by ~ 100) and near the minimum T_1 varies by factor 10 (T_2 by factor 1.0). The experimental data cannot be described in terms of a single thermal activation energy or the classical vacancy motion. We therefore included a quantum tunneling term analogous to that proposed by Ebner and Sung[27] to obtain an accurate quantitative fit. The best fit was obtained using

$$\lambda(T)\omega_1(T) \propto e^{-91/T}\{1 + 5.1 \times 10^4 e^{-107/T}\} \tag{74}$$

For this fit the formation energy $\Phi = 91\mathrm{K}$ and the potential barrier height $V = 107\mathrm{K}$. Note that the total activation energy is in agreement with earlier studies.[31–34,36,56] The prefactor of the classical diffusion constant is given by $D_0^{class} = 4.8 \times 10^{-3}\ \mathrm{cm}^2/\mathrm{sec}$ which is also in good agreement with previous determinations (see Table VII). The calculated T_1 values for classical vacancy diffusion alone is shown by the broken line of Fig. 33. In addition to the vacancy motions the experimental results also indicate the possibility of particle-particle tunneling at low temperatures and thus must be taken into account to obtain a complete analysis of the data.

In order to obtain the fits shown in Fig. 33 for the full temperature range we used the same model as that invoked to describe the behavior of ^{3}He impurities in solid ^{4}He [1-3,5,61-63] and recent results for T_2 studies of HD in solid H$_2$ [46-48]. The low temperature relaxation is attributed to particle-particle quantum exchange of impurity particles (HD molecules) with host molecules (para-H$_2$).

Because of their tunneling, the HD impurities are delocalized and are believed to propagate as wave-like excitations (impuritons) at low temperatures. Recent T_2 studies[46-48] of HD molecules in solid H$_2$ have also been interpreted in terms of impurity- particle exchange. HD particles travel through the lattice in the same manner as the vacancies, but with much smaller exchange frequencies. The relaxation occurs via the modulation of the magnetic interaction between the HD molecules and the ortho- H$_2$ molecules when the former are scattered by the elastic deformation field around the effectively static ortho-H$_2$ molecules. The cross relaxation rate is given by

$$\frac{1}{T_2^{ab}} = \frac{2}{9} M_2^{ab}(X)/J_{eff} \tag{75}$$

where the effective exchange frequency is related to the microscopic exchange rate J by [14]

$$J_{eff} = J_x(U_0/J)^{\frac{1}{n}} \tag{76}$$

for a scattering interaction potential

$$U(R) = U_0(a_0/R)^{3/n} \tag{77}$$

As a result of their tunneling, the HD impurities are believed to be delocalized by the 3- particle cyclic permutations at low temperatures. The minimum in T_1 occurs because on warming above 7K the coherent motion of the impurities is interrupted by scattering of vacancies rather than by the ortho-H$_2$ impurities. The temperature at which this crossover occurs can be estimated from the condition that the effective scattering by vacancies becomes comparable to that by ortho-H_2 molecules. This occurs where

$$X_v(T)\omega_v \gtrsim X_{ortho}J \tag{78}$$

where $X_v(T)$ is the density of vacancy, ω_v is the tunneling frequency of vacancies, X is the concentration of ortho-H_2 and J is the tunneling frequency of HD impurities. We find that this will happen at $T \gtrsim 8$ K in good agreement with the experimental result (Fig. 33).

When the vacancy scattering mechanism becomes effective J^{-1}_{eff} must be replaced by [62]

$$J^{-1}_{scatt}(T) = J^{-1}_{eff} + \omega^{-1}_{IV}(T) \tag{79}$$

where $\omega_{IV} = \frac{2\pi}{3}J^2/X_v(T)\omega_v(T)$ is the impurity vacancy scattering rate.[62] The overall temperature dependence for both the vacancy motion and impurity motion is given by

$$\frac{1}{T_1^{HD}} = \frac{2f}{9}M_2^{eff}(X)J_{20}(0) \tag{80}$$

with

$$J_{20}^{-1}(0) = 4[X_v(T)\omega_v(T) + J_{scatt}(T)] \tag{81}$$

The fit over the full temperature range given by the solid line of Figure 33 was obtained using this spectral density and the modulation frequency of equation

$$\omega_D = 2Z\sqrt{\frac{2\pi}{15}}X_v(T)\omega_v$$

$$= 4.4\times10^9 e^{-91/T}[1+5.1\times10^6 e^{-107/T}] \tag{82}$$

The use of only a single activation energy does not describe the temperature dependence over the full range (see Fig. 34) and we conclude that both the

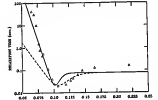

Figure 34 Comparison of the observed temperature dependence of the nuclear spin-lattice relaxation of HD impurities (1.1%) in solid H_2 (1.8 – 2.1% ortho) with the calculated dependance for single activation: solid line $E_A = 198$ K, broken line $E_A = 91$K. The observed relaxation is attributed to cross-relaxation between the HD impurities and the ortho-H_2 molecules.

quantum tunneling term and the classical activation term in equation (82) are needed to describe the complete behavior.

The use of the value of the exchange frequency $(J/2\pi)$ determined from the T_2 studies[46] to describe the low temperature regime gives a qualitatively good fit except at low temperatures where we observe an approximately linear increase in T_1 as a function of T^{-1} from 6K to 1K. In this temperature range the ortho H_2 line width increases because of the slowing down of the molecular reorientations and the number of ortho-H_2 molecules on "speaking terms" with the HD molecules is reduced. This occurs because at low temperatures the ortho- molecules form pairs whose NMR spectrum covers 43 KHz, which is much greater than that of the isolated ortho molecules. This in turn reduces the cross-relaxation rate and can be estimated by determining the overlap factor for the two spin species in the formulation of the two-bath relaxation scheme. Using the method developed by Weinhaus *et al* [31] for solid D_2, we obtained an improved fit in the Fig. 35 for our para hydrogen sample (with 1.8% ortho-H_2 and 1.1% HD impurities).

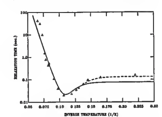

Figure 35. Correction (as dash line) of calculated temperature dependence of relaxation at low temperatures to account for the broadening of the ortho H_2 line shape relative to the HD line-shape.

Table VII Values of the Parameters in the Diffusion Constant

$$D = e^{-\Phi/T}[D_0^{qu} + D_0^{class} e^{-V/T}]$$

Ref	Φ (K)	V (K)	$\Phi + V$ (K)	D_0^{qu} cm^2/sec $\times 10^8$	D_0^{class} cm^2/sec $\times 10^3$
Expt.					
*	91 ± 6	107 ± 3	198 ± 6	3.8	4.9
18	91 ± 10	104 ± 5	195 ± 10	1.9	5.1
9	—	—	191	—	—
11	—	—	198	—	3.8
12	—	—	200 ± 10	—	3.0
Theory					
8	112	85	197	200	0.6

* This study

3.5 Pressure Dependence of T_2

Several 1.1% HD samples with different ortho concentrations (e.g. 2.1%, 1.8%, 0.5% ortho-H_2) were pressurized using ^{4}He. Liquid helium was condensed directly on top of the H_2 sample and the pressure read by a pressure gauge (Heise Model 45441) external to the cryostat. The converter pot and the fill line above the pot were heated above 2K to prevent solidification of the ^{4}He for applied pressures $P > 25$ bar. A pressure detector was mounted directly on one end of the NMR cell to verify that the pressure was transmitted to the sample even when the fill line at the entry to the NMR cell contained solid ^{4}He.

Let us now discuss the para hydrogen sample with 0.5% ortho-H_2 and 1.1% HD molecule first (Fig. 32). At low temperature $0.1 < T < 6.5$K T_2 is essentially independent of temperature and significantly longer than the rigid lattice value. For dilute HD concentrations, the value of T_2 for the rigid lattice according to the statistical theory is $(T_2)_{rigid} = 8.2X^{-1} \times 10^{-6}$ sec [11,56] where X is the ortho concentration. Treating the HD molecules as fixed, randomly distributed spin $\frac{1}{2}$ nuclei as far as the relaxation is concerned, we find for a rigid lattice of 1.1% HD and 0.5% ortho-hydrogen

$$(T_2)_{rigid} = 0.90 \; msec \tag{83}$$

which is to be compared to the observed value

$$(T_2)_{expt} = 3.43 \pm 0.07 \; msec \tag{84}$$

at $P = 0$. At the lowest temperatures, we observed a small approximately linear increase in T_2 on cooling for $0.1 < T < 0.7$K, with $\Delta T_2/T_2\Delta T \approx 0.30\text{K}^{-1}$. This is believed to be associated with the quenching of the rotational degrees of freedom of the ortho molecules at low temperatures. Only part of the broadened ortho H_2 NMR spectrum is then on speaking terms with the HD spectrum and the relaxation rate T_2^{-1} is decreased.

At high temperatures, T_2 is observed to pass through a minimum of 2.46 ms at $T \approx 8.3$K, and then to increase exponentially with temperature for $9.5 < T < 13.5$K. The latter behavior has been interpreted in terms of the formation of mobile vacancies which enhance the relaxation rate as one approaches the melting point.

The value of T_2 were observed to decrease smoothly with applied pressure decreasing to 2.44 $msec$ for $P = 136$ bar (see Table VIII). The pressure dependence appears to be saturate for $P = 150$ bar and suggest a limiting value $T_2' \approx 2.30 msec$, which is significantly higher than the calculated rigid lattice value. The pressure dependence observed for different ortho concentrations $x = 0.5, 2.1$[46] and 1.8% are similar with that we observed in this sample. At low temperatures $T = 230$ mK we observed a change in T_2, 3.1 to 2.4 *msec*[46] for $\Delta P = 20$ bars for another sample. The change is much larger than the 0.9% effect expected for a rigid lattice, using the experimental compressibilities.[13] The Gruenesen constant[11]

$$\Delta \ln T_2 / \Delta \ln V \approx 28 \tag{85}$$

is comparable to that observed for quantum tunneling in solid helium.

The pressure dependence of T_2 is less than that predicted by the simple model of Delrieu and Sullivan[11] and could be understood in terms of a 20% – 30% overestimation of the free volume of the exchanging particles. This is possible because (1) HD molecules in para hydrogen create a strain field (distortion field) to decrease the free volume between the HD impurities and the surrounding para hydrogen and (2) the volume/mole of solid HD 20.57 cc/mole is smaller than the volume/mole of solid H_2 23.16 cm/mole[13,64–66] and therefore the volume/mole of the samples of para hydrogen with HD impurities are smaller than pure para hydrogen. Therefore the compressabilities of para hydrogen with HD impurities are smaller than the pure para hydrogen. It can be understood that the tunneling frequency of HD molecule is less than the tunneling frequency of pure para hydrogen (at the same order ~ 1 KHz) and that the tunneling frequency of HD molecules is less sensitive to the pressure. This could be proved by experiments as follows:

(1) The density and compressibility measurements of para hydrogen sample with HD impurities.

(2) T_2 measurements in the very dilute HD concentration (e.g. $X_{HD} = 0.1\%$, $X_{ortho} = 0.1\%$ and 0.5%) para-hydrogen samples: the tunneling frequency

of HD molecules will be higher than present sample (1.1% HD, 0.5% ortho) and will be more pressure dependent. The temperature dependences observed for different ortho concentrations $x = 0.5$, 2.1, and 2.5% are all similar and scale linearly with ortho concentration.[46] We have analyzed the data using the theory of Kubo and Tomita[67] who calculated the dependence of the secular half width of the NMR absorption of the correlation time T_c of the local fields. This results in

$$(\frac{1}{T_2})^2 = \frac{2}{\pi}(\frac{1}{T_2})^2_{RL}\tan^{-1}(\frac{\pi\tau_c}{4\ln 2T_2}) \tag{86}$$

where the rigid lattice value is related to the second moment M_2 by

$$(\frac{1}{T_2})_{RL} = (2\ln 2M_2)^{1/2} \tag{87}$$

(see asymptotic limit of Fig. 2 of Ref. 67). Using their result, we can determine the characteristic motional frequency τ_c^{-1} using

$$M_2^{\frac{1}{2}}\tau_c = \frac{2}{\pi}\sqrt{2\ln 2}\frac{T_2}{(T_2)_{RL}}\tan[\frac{\pi}{2}(\frac{(T_2)_{RL}}{T_2})^2] \tag{88}$$

The values of $M_2^{\frac{1}{2}}\tau_c$ obtained from this analysis using $(T_2)_{RL} = 2.3$ ms (the limiting value observed experimentally) are given as a function of molar volume in Table VIII and Fig. 36.

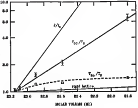

Figure 36 Comparison of the volume dependence of the calculated exchange frequency J/J_0 the observed relaxation time T_{20}/T_2, the characteristic motional frequency τ_{c0}/τ_c deduced from the values of T_2 and the variation for a rigid lattice The index 0 refers to the values at $P = 0$

Table VIII. Volume dependence of relaxation time T_2, the calculated three-particle exchange frequency J, the parameter φ (see text), the bulk modulus B and the motional frequency τ_c^{-1} deduced from T_2 using the theory of Kubo and Toyota.

	P (bar)	V_m (cm^3)	T_2 (ms)	$M_2^{1/2}\tau_c$	B (bar)^a	φ	J (kHz)	τ_c^{-1} (kHz)
experiment	0.0	23.15	3.43	0.97^b				0.814
	3.6	23.10	3.20	1.08				0.731
	20.1	22.90	2.80	1.61				0.491
	46.0	22.56	2.72	2.04				0.387
	136.0	21.80	2.47	6.45				0.122
theory	0	23.15			1861	26.6	9.52	
	20	22.90			2000	28.6	4.70	
	40	22.69			2150	30.7	2.20	
	60	22.48			2200	32.3	1.34	
	100	22.10			2520	36.1	0.398	
	140	21.77			2780	39.7	0.133	

^{a} The bulk moduli are taken from Ref. 48. ^{b} For $M_2^{1/2} = 790$ Hz, we find $\tau_c^{-1} \approx 814$ Hz (at $P = 0$) which is an order of magnitude smaller than the calculated values of J.

The observed volume dependence for τ_c is very much greater than that expected for a rigid lattice ($\Gamma_{RL} = \partial \ln T_2 / \partial \ln V_m = 2$) but it is appreciably weaker than that given by the calculations[11] of Delrieu and Sullivan. This can be understood in terms of difference between the HD molecule and the para H_2 molecule as we discussed above.

In order to compare the observed volume dependence with the calculated values, we have in Fig. 36 plotted the normalized values J_0/J, τ_c/τ_{c0} and T_{20}/T_2 where the index 0 refers to the value at $P = 0$. The Grüneisen constants are $\Gamma_J = 63.6$, $\Gamma_{\tau_c} = -31.4 \pm 3.0$ and $\Gamma_{T_2} = 11.6 \pm 1.0$. The volume dependence is clearly much stronger than that of a rigid lattice, and any interpretation of the results in terms of rigid lattice spin spin interactions appears to be excluded.

The difference between Γ_J and Γ_{T_c} could be accounted for in terms of an overestimation of the compressional energy δU. It is possible that the volume dependence of δU will be appreciable softened by the strain field around HD molecules and the density change caused by the difference between the HD impurities and para hydrogen matrix. There is need for a more detailed theory of this effects, and they should be tested for very dilute ($\sim 0.1\%$) **HD** and very dilute ($x < 0.5\%$) ortho- H_2 samples.

5.6 Clustering of the Ortho H_2

The "aging" effect of the relaxation time has been observed in this work which is consistent with the previous work of Duke University. The values of T_2 of a freshly grown sample, cooled below 1K for the first time is observed to increase by a factor of approximately 2.5 over a 48 hour time scale. This is attributed to the very slow clustering of ortho molecules into pairs. Because the quadrupole-quadrupole interaction to ortho align in a stable low energy Tee configuration (axes mutually perpendicular) each ortho molecule then has a well defined intramolecular interaction which results in a fine structure splitting of the ortho H_2 line into a doublet with ±43 kHz separation on the Larmor frequency. The HD spectrum is now no longer on "speaking terms" with the ^{1}H spectrum of the ortho pairs and the $I_1^+ I_2^-$ components of the HD ortho H_2 dipolar interactions is no longer effective. The linewidth (T_2^{-1}) is correspondingly decreased by a factor of 4/9. This is close to the observed trend.

CHAPTER 6

SUMMARY AND CONCLUSIONS

Solid hydrogen is a remarkable subject for study from both the theoretical and experimental viewpoint. The origin of this interest is that both the translational and the orientational degrees of freedom must be treated quantum mechanically in order to properly understand the fundamental properties of the solid hydrogen at low temperatures. The molecular centers of mass are only weakly localized with respect to quantum fluctuations because of the relative weak binding forces and the small molecular mass. The *rms* deviation $\langle U^2\rangle^{\frac{1}{2}}_{H_2} \approx 0.16R_0$ where R_0 is the nearest neighbor separation.[5,13] As a result of this zero point motion, there is an appreciable overlap of the wave functions of molecules on neighboring lattice sites and this allows defects such as isotopic impurities (HD) and vacancies to exchange positions with nearest neighbor para H_2 molecules in the para hydrogen crystal (i.e., low concentration ortho H_2 and low concentration HD impurities). Impurity tunneling of this kind has been reported[2,3,61,68] for ^{3}He impurities in solid *hcp* ^{4}He where the quantum delocalization is significantly higher than is found for solid H_2, $\langle u^2\rangle^{\frac{1}{2}}_{^4He} \approx 0.30R_0$ (at the lowest density). Analyses of the detailed structures of the nuclear magnetically ordered states in solid ^{3}He have led to the conclusion that there are significant three- and four-particle cyclic permutations in addition to two-particle permutations.[9] The extension to solid para hydrogen (another family member of the quantum crystals) of the multiple-particle exchange model and more detailed calculations were carried out by Delrieu and Sullivan[14] in which the multiple particle exchange process can be understood if the exchange rate is determined by the available free volume for permuting the particles in the solid para hydrogen. This model predicts an unexpectedly large three particle exchange rate (at the order of 1 KHz) in *hcp* para H_2 at normal densities ($P = 0$), decreasing to ~ 100 Hz for applied pressures $P = 100$ bar.[11] Earlier models[22] based on two-particle exchange calculated from the overlap of Gaussian wave functions predicted $J \sim 10^{-1} - 10^{-4}$ Hz. The difference in 4 orders of magnitude of the tunneling frequency of para-H_2 (represented by HD impurity) provides a severe test to the multiple cycle exchange model. Previous experiments have shown that the NMR line-width of the HD impurities is smaller (by a factor of approximately 5) than the calculated rigid lattice linewidth.[46] It therefore became important to determine the tunneling frequency of HD impurities and the pressure dependence of the HD line shape for the solid para hydrogen in order to distinguish between motional narrowing due to tunneling and any possible uncertainties in the calculation of the linewidth.

In the same manner as HD impurities, the vacancies in para H_2 solid travel through the lattice with much higher exchange frequencies, because of the low activation energy which is typically three orders of magnitude higher than particle-particle exchange rates.[6,29,69,70] Vacancies exist in the solid para hydrogen at finite temperatures. The concentration of vacancy

$$X_v \propto e^{-\Phi_v/k_B T} \tag{89}$$

where Φ_v is the formation energy of vacancy. Because of the existence of two bound states of the vacancy[27] there exist two different kinds of vacancy motions as follows: (1) classical hopping over the potential barrier which dominates the high temperature domain and (2) the quantum tunneling which conserves energy (the activation energy is just Φ_v, the vacancy formation energy) and which should dominate the vacancy motion at low temperature domain.

Therefore the diffusion constant for the quantum crystal will in general be of the form

$$D(T) = e^{-\Phi_v/k_BT}[D_0^{qu} + D_0^{class}e^{-V/k_BT}] \tag{90}$$

where D_0^{qu} is the diffusion constant of quantum tunneling, D_0^{class} is the diffusion constant of classical hopping, V is the potential barrier.

A single activation energy will not be a adequate over the full temperature range. Ebner and Sung[27] have estimated that the crossover from classical activation to quantum tunneling will occur for vacancies in solid H_2 below approximately 14K, but this was not seen in earlier studies.[31–34,36,37,56]

The presence of quantum tunneling can be determined by comparing NMR studies with x ray measurements. X ray studies measure vacancy concentrations $X_v(T) = \exp(-\Phi_v/k_BT)$ while NMR studies measure the product $X_v(T)\omega_v(T)$ where $\omega_v(T)$ is the characteristic motional frequency for the vacancies. $X_v(T)\omega_v(T)$ varies as $\exp[-(\Phi + V)/k_BT]$ for classical activation and as $\exp[-\phi_v/k_BT]$ for quantum tunneling. Such a comparison for bcc ^3He has led to the conclusion that vacancies move by quantum tunneling in low density solid ^3He.[69–71]

In addition to testing the multiple exchange model the second aim of this dissertation is to present new data for vacancy-induced nuclear spin lattice relaxation in solid para hydrogen (low ortho concentration ~ 1%). The experimental conditions were chosen so that the vacancy motion could be studied at temperatures significantly lower than those of previous investigations at high frequencies (208 MHz) which provided a better sensitivity and thus test for the existence of quantum tunneling at lower temperatures.

In conclusion, measurements of the nuclear spin–spin relaxation times T_2 of HD impurities in carefully annealed crystals of para hydrogen show strong evidence for the existence of quantum tunneling in solid H_2 via exchange (3–particle cyclic permutation) with nearest–neighbor molecules. T_2 is essentially temperature independent at low temperatures (corresponding to a motionally narrowed line shape a factor of 5.4 smaller than the rigid lattice value) and passes through a minimum at approximately 9.2K, which is attributed to scattering by vacancies (or phonons) which interrupts the coherent quantum tunneling of the HD impurities. The tunneling frequency of HD impurities in solid para hydrogen is found to be $J_t = 1.54$ kHz ± 0.08 kHz which is consistent with the prediction that J_t is at the order of magnitude of 1 kHz by the calculation provided by Delrieu and Sullivan[11] who extended the multiple cyclic exchange model to the solid para hydrogen. The pressure dependence measurements of the nuclear spin–spin relaxation time T_2 of HD impurities in solid H_2 show evidence of motional narrowing which is strongly pressure dependent. A 29% decreasing (0.0% for rigid lattice) of T_2 (related to tunneling frequency) is observed by an applied pressure $P = 136$ bar in comparison with the T_2 value of $P = 0$ bar in a para hydrogen sample (0.5% ortho, 1.1% HD). In consistency with the above measurement, a 23% decrease (0.5% for rigid lattice) of T_2 is observed for a different sample (2.1% ortho, 1.1% HD) at $P = 20$ bar in comparison with $P = 0$ bar, which is much larger than the 0.3% effect expected for a rigid lattice using the experimental compressibilities.[13] Therefore, any rigid lattice model is unable to explain the quantum effect of HD impurities in solid para hydrogen. The Grüneisen constants ($\Delta \ln T_2/\Delta \ln V$) are 31 and 28 respectively for the above two samples which is comparable to that observed for quantum tunneling in solid helium.

The pressure dependence for T_2 is less than that predicted by the simple model of Delrieu and Sullivan which may be understood in terms of a 20% - 30% overestimate of the free volume of the exchange particles. This calculation may be improved by considering the following.

(1) The HD impurities in a para-hydrogen matrix form a strain field (distortion field) to decrease the free volume between the HD impurities and the surrounding para hydrogen. The tunneling frequencies of HD impurities are therefore slightly smaller than the tunneling frequencies of para hydrogen molecule at the same order of magnitude.

(2) The volume/mole of solid HD is smaller than solid para hydrogen and therefore the para hydrogen sample with HD impurities is denser than the pure para hydrogen without HD impurities at $P = 0$. Hence, the pressure dependence of the compressibility of the sample with impurities will be smaller than that of a sample without HD impurities (with the same concentration of ortho-H_2). This can be used to understand why the pressure dependence observed is lower than the prediction of Delrieu and Sullivan. The details of this need to be pursued theoretically.

To test this modification to the calculations of Delrieu and Sullivan, we suggest that T_2 measurements and pressure dependence tests may need to be carried out at very dilute (e.g., 0.1% HD and 0.1% - 0.5% ortho) para-hydrogen sample.

We have also found that the concentration (ortho-H_2) dependence of T_2 is consistent with the theory. The temperature dependences observed for different ortho concentrations $x = 0.5, 2.1$ and 2.5% are all similar and scale linearly with ortho concentration and have been reported elsewhere.[46]

A very weak but smooth temperature dependence is seen at low temperatures with T_2 increasing from 1.7 to 2.6 *msec* as T is lowered from 4.5 to 0.16K. This is not quantitatively understood but any thermal process that destroys the coherent motion of the impurities would account for this weak temperature dependence

APPENDIX A

LOCAL ORDERING IN DILUTE ORTHO PARA HYDROGEN MIXTURES AT LOW TEMPERATURES

We have carried out a systematic investigation[70–72] (Fig 37 and Fig 38) of the temperature dependence of the orientational degree of freedom and the variation of the "glass order parameter" for dilute solid ortho–para mixtures down to low temperatures

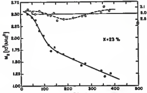

Figure 37 Temperature dependence of the intramolecular second moment M_2 for an ortho concentration $X = 23\%$ (above percolation) (The solid and broken lines serve only as guides to the eye)

The results indicate that there is a progressive freezing of the orientational degrees of freedom of the ortho-H_2 molecules as the samples are cooled. The qualitative picture of a glasslike phase with both the local symmetry axes and the

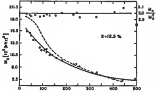

Figure 38 Temperature dependence of the intramolecular second moment M_2 for an ortho concentration $X = 12.5\%$ (below percolation). The sample is the same as that for Figure 11, but aged at low temperatures. The broken line refers to the dependence seen for $X = 23\%$ but scaled to match the 12.5% data at 350 mK assuming a simple $X(1-X)$ dependence

local alignments σ varying from site to site is essentially correct. No evidence is seen for any static phase transition into an orientational glass phase analogous to the spin glasses, and this is attributed to the fact that the local symmetry is broken even in the completely disordered (para- orientational) phase by the replacement of the ortho molecules with the spherically symmetric para molecules. The results indicate a weak collective ordering for concentrations above percolation which is absent for low concentrations.

APPENDIX B

UNUSUAL LOW-TEMPERATURE EFFECT ON THE NMR LINE SHAPES IN SOLID HYDROGEN

The NMR absorption line shapes in solid hydrogen develop a distinctive asymmetry in the presence of an appreciable nuclear spin polarization.[73] This asymmetry has been analyzed quantitatively and it is shown that the effect of nuclear polarization needs to be taken into consideration in order to obtain a reliable determination of the molecular orientational-order-parameter distribution. The intensity of an NMR absorption line depends on the population difference of adjacent Zeeman levels while the frequency of absorption is given by the splitting between those levels. Ortho H_2 has three Zeeman levels corresponding to $I = 0, \pm 1$, and therefore two NMR absorption lines. The relative intensity of these two transitions is given by

$$\frac{I_{1,0}}{I_{0,-1}} = \exp(-\hbar\omega_0/k_B T) \tag{91}$$

where $\hbar\omega_0$ is the level splitting and ω_0 is the Larmor frequency. In the high temperature limit $k_B T >> \hbar\omega_0$ the two transitions are of equal intensity and each intensity is inversely proportional to the temperature (the "nuclear Curie Law"). At high spin polarizations, however, the intensities are no longer equal and if the frequencies are different this can be seen experimentally (Fig. 39, Fig. 40 and Fig. 41).

These conditions are satisfied for solid H_2 at low temperatures. The splittings between the Zeeman levels are perturbed by the intramolecular nuclear dipole-dipole interactions. If the molecules are free to rotate (at high temperatures)

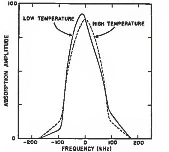

Figure 30 Calculated NMR absorption lines shapes in solid H_2 for a non trivial nuclear spin polarization P The solid line represents $P = 50\%$ The broken line represents $P < 1\%$ Both curves are normalized to the same area for the sake of comparison

the intramolecular interactions average to zero and only a single line is present in the absorption spectrum. At low temperatures, however, the ortho-H_2 molecules orient themselves along local symmetry axes to minimize their interaction energy

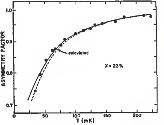

Figure 40. Asymmetry factor (A convenient measure of the intensities at the maximum positive and negative slopes of the line shape.) for $X = 23\%$. The solid curve gives the calculated values ignoring temperature gradients. The dashed curve illustrates the variation for a thermal gradient $\nabla T = 8$ mK/D at 46 mK (for a sample geometry with $D = 0.1$ mm)

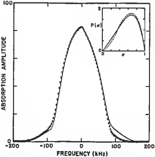

Figure 41 Comparison of observed asymmetrical line shape (+) with the calculated shape (solid line) for the order parameter distribution $P(\sigma)$ shown in the inset The broken line in the inset refers to the $P(\sigma)$ deduced in earlier work (Ref 74) which neglected polarization effects

REFERENCES

1 A.F Andreev and I.M Lifshitz, *Zh Eksp Teor Fiz* **56** 2057 (1969) [*Sov Phys JETP* **29** 1107 (1969)]

2 A.R Allen and M.G Richards *Phys Lett* **65A** 36, (1978)

3 A R Allen, M G Richards and J Schratter *J Low Temp Phys* **30** 137 (1978)

4 L H Nosanow *Phys Rev Lett* **8** 164 (1966)

5 R A Guyer, *Solid State Phys* **23** 413 (1969)

6 A Landesman *Ann Phys* (Paris) **9** 53 (1969) **9** 69 (1975) *J Low Temp Phys* **30**, 117 (1978)

7 W P Kirk and E D Adams, *Phys Rev Lett* **27** 392 (1971)

8 J H Hetherington and F.D C Willard *Phys Rev Lett* **35** 1442 (1975)

9 M Roger J H Hetherington and J M Delrieu *Rev Mod Phys* **55** 1 (1983)

10 M Roger *Phys Rev B* **30** 6342 (1984)

11 J M Delrieu and N S Sullivan, *Phys Rev B* **23** 3197 (1981)

12 G C Straty and E D Adams *Phys Rev* **169** 232 (1968)

13 F Silvera *Rev Mod. Phys* **52** 191 (1980)

14 A Abramowitz and I A Stegun, *Handbook of Mathematical Functions* (Dover, New York, 1972)

15 N S Sullivan and R.V Pound *Phys Lett* **39A** 22 (1972)

16 N S Sullivan, H Vinegar and R V Pound *Phys Rev B* **12** 2596 (1975)

17 R R Feynman "*Statistical Mechanics*" A set of lecture notes taken by R Kikuchi and H A Feiveson, edited by Jacob Shaham (1972)

18 R Schweizer S Washburn and H Meyer *J Phys* (Paris) **39** C6 95 (1978) *Phys Rev Lett* **40** 1035 (1978)

19 J H Constable Ph D Thesis (Ohio State University 1969) (unpublished)

20 M H Kalos, D Levesque and L Verlet *Phys Rev A* **9** 2178 (1974)

21 R A Guyer, R C Richardson and L I Zane *Rev Mod Phys* **43** 532 (1971)

22 R Oyarzun and J Van Kranendonk *Can J Phys* **50** 149 (1972)

23 R Wanner and H Meyer *J Low Temp Phys* **11** 715 (1973)

24 N S Sullivan, *Bulletin of Magnetic Resonance VII*, 1/2 (1987) "Quantum Crystal," A set of lecture notes at the University of Florida (1984 1986) unpublished

25 J E Sacco, A Widom D Lorke and M G Richards *Phys Rev Lett* **37** 760 (1978)

26 C M Edwards D Zhou and N S Sullivan, *Bull Am Phys Soc* **32** 512 (1987), *Physica* **T19B** 458 (1987)

27 C Ebner and C C Sung *Phys. Rev A* **5**, 2625 (1972).

28 D Zhou M Rall J P Brison and N S Sullivan "Vacancy Induced Nuclear Spin lattice Relaxation in Solid H_2 " submitted to *Phys Rev B*

29 A Landesman *Ann Phys* **9**, 69 (1975) *J Low Temp Phys* **17** 365 (1974) **Vol 2** p 115

30 A Abragam and M Goldman in *Nuclear Magnetism Order and Disorder* Oxford University Press Oxford 1982 Chapter 3

31 F Weinhaus and H Meyer *Phys Rev B* **7** 2974 (1973)

32 F Weinhaus, H Meyer S M Myers and A B Harris *Phys Rev B* **7** 2960 (1973)

33 M Bloom *Physica* **23** 767 (1957)

34 A B Harris, *Phys Rev B* **2** 3495 (1970)

35 A Abragam in *Principles of Nuclear Magnetism* (Clarendon Press Oxford 1961) Chapter X

36 G W Smith and C F Squire *Phys Rev* **111** 188 (1958)

37 W P A Hass N J Poulis and J J W Borleffs *Physica* **27** 1037 (1987)

38 Y S Kim, J S Park C M Edwards and N S Sullivan *Cryogenics* **27** 438 (1987)

39 G K White *Experimental Techniques in Low Temperature Physics*, Oxford University Press Oxford 1979

40 Model CGR 1-3000 Lake Shore Cryotronics, Columbus OH 43229

41 M Rall "Tunneling in Quantum Solids NMR Studies on Solid Hydrogen" Master's thesis University of Florida 1978 unpublished

42. L Fredericks C M Edwards and N S Sullivan Design of UHF Q meters 1984 unpublished

43 N.S Sullivan and R.V Pound *Cryogenics* **13** 28 (1973)

44 N S Sullivan, D Zhou and C M Edwards, "Precise and Efficient *In Situ* Ortho–Para–Hydrogen Converter," submitted to *Cryogenics*

45 C M Edwards D Zhou and N S Sullivan, *Physica Scripta* **T19B** 486 (1987)

46 D Zhou C M Edwards and N S Sullivan, *Phys Rev Lett* **62** 1528 (1989)

47 D Zhou M Rall N S Sullivan, C M. Edwards and J P Brison, *Solid State Comm* **72, 7** 657 (1989)

48 N S Sullivan, D Zhou, M Rall and C M Edwards, *Phys Lett A* **138 6,7** 329 (1989)

49 Model CGR 1 3000, Lake Shore Cryotronics, Columbus, OH 43229

50 As reported *in* Figure 1 of C C Sung *Phys Rev* **167** 275 (1968)

51 D Esteve M. Devoret and N S Sullivan, *J Phys C* (Solid State) **15** 5455 (1982)

52 N S Sullivan M Devoret B.P Cowan and C Urbina *Phys Rev B* **17** 5016 (1978)

53 S Washburn R Schweizer and H Meyer *J Low Temp Phys* **40** 1036 (1980)

54 R Schweizer S Washburn and H Meyer *Phys Rev Lett* **40** 1036 (1978)

55 I Yu, *J Low Temp Phys* **40** 625 (1985)

56 R F Buzerak M. Chan and H Meyer *J Low Temp. Phys.* **28** 415 (1977)

57 A Landesman, *J Low Temp Phys* **30** 117 (1978)

58 D I Pushkarov *Pis'ma Zh Eksp Teor Fiz* **19** 751 (1974) [*JETP Lett* **19** 386 (1974)

59 T McMullen, *J Low Temp Phys* **38** 619 (1980)

60 A E Stillman L J Schwartz and J.H Freed, *J Chem Phys* **73** 3502 (1980)

61 M G Richards J Pope and A. Widom *Phys Rev Lett* **29** 708 (1972) **37** , 760 (1976)

62 D P Locke, *J Low Temp Phys* **32** 159 (1978)

63 V N Grigorev B N Esselson V A Mikheev V A Slusarev M S Strzhemechny and Y E Schulman *J Low Temp Phys* **13** 1965 (1973)

64 L F Silvera A Driessen and J A deWaal, *Phys Lett A* **68** 207 (1978)

65 A Birnbaum and J D Poll *J Atmos Sci* **26** 943 (1969)

66 O Bostanjoglo and R Kleinschmidt *J Chem Phys* **46** 2004 (1967)

67 R Kubo and K Toyabe *J Phys Soc Japan* **9** 888 (1954)

68 Y Hirayoshi T Mizusaki S Maegawa and A Hirai *J Low Temp Phys* **30,** 137 (1978)

69 N S Sullivan, G Deville and A Landesman, *Phys Rev* B **11,** 1958 (1975)

70 M E R Bernier and J H Hetherington *Phys Rev* **39,** 11285 (1980)

71 S.M Heald, D.R. Bear and R O Simmons, *Phys Rev B* **30,** 2531 (1984)

72. C M Edwards D Zhou Y Lin and N S Sullivan, *J Low Temp Phys* **72, 1/2** 1 (1988)

73 D Zhou C M Edwards and N S Sullivan, *Solid State Commun* **60, No. 12** 901 (1986)

74 N.S Sullivan C M Edwards Y Lin and D Zhou *Can J Phys.* **65** 1463 (1987)

75 C M. Edwards, D Zhou and N S Sullivan *Phys Rev* B **34** 6540 (1986)

76 R V Pound and N S Sullivan *Cryogenics* **13,** 28 (1973)

BIOGRAPHICAL SKETCH

Dowei Zhou is a graduate of Beijing Fourth Middle and High School of China. He passed the National Entrance Examination and was admitted by Qinghua University (Beijing), which is one of the best engineering universities in China. He graduated in 1970 with a major in metallurgy and mechanism from Qinghua University.

From 1970 to 1978, he worked as an engineer in the Xingtai Steel and Iron Factory and in the experimental factory of the Chinese Academy of Sciences of Railways. During that period he designed, repaired, constructed and installed some machines and iron-smelting furnaces; he also worked on smelting different alloys and casting. He was admitted to North Transportation University to study electrical engineering for one year from 1978 to 1979. He was then admitted as a graduate student by the Graduate School of the Chinese Academy of Sciences and the Beijing Physics Institute of the Chinese Academy of Sciences after he passed the Graduate Entrance Examination in 1979. His advisor, Guan Wei Yan, was a well-known researcher in superconductivity and was a graduate student of Kapitza. Mr. Zhou's master thesis title was "The Effect of H Ion Implantation to the Rapidly Quenched Al-Si Alloy Superconductors." During that time he received six admissions with fellowships or assistantships from graduate schools in the United States. He accepted admission at the University of Florida because he knew that this university was on the top level of the low temperature physics research. The day after he defended his master's thesis, January 20, 1982, he flew to the United States and then landed in Gainesville, Florida.

Mr. Zhou started part-time research in Dr. N. S. Sullivan's laboratory in the fall of 1984, and after passing the qualifying examinations, he was kindly admitted to Dr. Sullivan's research group. Since then, he has mainly worked in the field of quantum tunneling in solid hydrogen under the direction of Professor Sullivan. Mr. Zhou said that the future is a long road, UF is his new starting point. He has made his stay at UF a pleasant and rewarding experience; he will never forget the spirit of devotion to science and the cooperative manner with colleagues and students at the University of Florida.

I certify that I have read this study and that in my opinion it conforms to acceptable standards of scholarly presentation and is fully adequate, in scope and quality, as a dissertation for the degree of Doctor of Philosophy.

NS Sullivan

Neil S Sullivan, Chair
Professor of Physics

I certify that I have read this study and that in my opinion it conforms to acceptable standards of scholarly presentation and is fully adequate, in scope and quality, as a dissertation for the degree of Doctor of Philosophy

ER Andrew

E Raymond Andrew
Graduate Research Professor of Physics

I certify that I have read this study and that in my opinion it conforms to acceptable standards of scholarly presentation and is fully adequate, in scope and quality, as a dissertation for the degree of Doctor of Philosophy.

E. Dwight Adams

E Dwight Adams
Professor of Physics

I certify that I have read this study and that in my opinion it conforms to acceptable standards of scholarly presentation and is fully adequate in scope and quality, as a dissertation for the degree of Doctor of Philosophy

J Robert Buchler

J Robert Buchler
Professor of Physics

I certify that I have read this study and that in my opinion it conforms to acceptable standards of scholarly presentation and is fully adequate, in scope and quality, as a dissertation for the degree of Doctor of Philosophy

Steph E Nagler

Stephen E. Nagler
Associate Professor of Physics

I certify that I have read this study and that in my opinion it conforms to acceptable standards of scholarly presentation and is fully adequate, in scope and quality, as a dissertation for the degree of Doctor of Philosophy

K N Scott

Katherine N Scott
Professor of Nuclear Engineering
Sciences

This dissertation was submitted to the Graduate Faculty of the Department of Physics in the College of Liberal Arts and Sciences and to the Graduate School and was accepted as partial fulfillment of the requirements for the degree of Doctor of Philosophy.

May 1990

Dean, Graduate School